

The Global Modal Parameterization for nonlinear model-order reduction in flexible multibody dynamics

Olivier Brüls¹, Pierre Duysinx² and Jean-Claude Golinval¹

¹LTAS-Vibrations et Identification des Structures, University of Liège,
Chemin des Chevreuils, 1, B52/3, B-4000 Liège, Belgium

²LTAS-Ingénierie des véhicules terrestres, University of Liège,
Chemin des Chevreuils, 1, B52/3, B-4000 Liège, Belgium

Abstract

In flexible multibody dynamics, advanced modelling methods lead to high-order nonlinear Differential-Algebraic Equations (DAEs). The development of model reduction techniques is motivated by control design problems, for which compact Ordinary Differential Equations (ODEs) in closed-form are desirable. In a linear framework, reduction techniques classically rely on a projection of the dynamics onto a linear subspace. In flexible multibody dynamics, we propose to project the dynamics onto a submanifold of the configuration space, which allows to eliminate the nonlinear holonomic constraints and to preserve the Lagrangian structure. The construction of this submanifold follows from the definition of a Global Modal Parameterization (GMP): the motion of the assembled mechanism is described in terms of rigid and flexible modes, which are configuration-dependent. The numerical reduction procedure is presented, and an approximation strategy is also implemented in order to build a closed-form expression of the reduced model in the configuration space. Numerical and experimental results illustrate the relevance of this approach.

Key-words: model reduction, component-mode technique, nonlinear projection, flexible multibody dynamics, parallel mechanisms.

1 INTRODUCTION

Facing the demand for faster, lighter and more accurate machines, the interest for complex flexible mechanisms with parallel topology has grown for several years in the fields of high-speed robots and machine-tools, large manipulators, space robots and foldable structures. Indeed, for a flexible mechanism, the bandwidth of motion is no more limited by the first natural frequency of vibration so that a lighter design and/or faster motions can be achieved. Parallel kinematic machines also have a higher stiffness and a reduced moving mass, since the actuators can be fixed to the base. Subsequent challenges arise for the control system, which has to deal with the flexible dynamics and the complex nonlinear kinematics in order to guarantee tracking performances, stability and disturbance rejection. The control design problem has to be solved using a dynamic model, which should ideally satisfy the following requirements.

1. Accuracy is needed in the bandwidth and in the workspace of interest.
2. A low-order model is usually necessary for the construction of a low-order controller.
3. Considering the large number of control techniques developed for various classes of nonlinear ODEs (e.g. Lagrangian, linear parameter varying, affine, passive, differentially flat

or two-time-scale systems), we look for closed-form and structured expressions which are free from algebraic constraints.

4. Computational efficiency is also critical for real-time implementation or for numerical optimization of a control law.
5. The formulation should be systematic for convenience and reliability.
6. Finally, the model should be easily exported to specialized control software.

Modern formalisms in flexible multibody dynamics allow a detailed and reliable representation of complex mechanical systems. However, high levels of accuracy and generality can only be reached at the price of sophisticated models, which require important computational efforts. For example, the nonlinear finite element approach [1, 2] is certainly one of the most general and systematic method, but the finite element parameterization involves a large number of redundant nodal coordinates, leading to a high-order numerical DAE model. Alternatively, the floating frame of reference approach [1, 3, 4, 5, 6] relies on a more compact parameterization, with a distinction between rigid and flexible coordinates, but in case of complex parallel mechanisms, the model is still represented by a rather large number of nonlinear DAEs.

A possible breakthrough may come from the combination of the nonlinear finite element method with a reduction technique, in order to build a simplified model with a minimized loss of accuracy. The control system is expected to be robust with respect to the omitted dynamics. Among reduction techniques, a distinction can be made between learning-based approaches, such as the method of Bottasso *et al.* [7] which involves the training of an artificial neural network, and projection methods, which are specifically addressed here. In the following review, we shall see that the projection can be defined either in the phase space (i.e. the state space) or in the configuration space.

1.1 Linear subspaces for linear systems

In linear system theory, a reduction procedure usually involves the construction of a subspace of the state space that contains the essential dynamics. Balanced truncation methods [8, 9, 10] rely on a singular value decomposition, and they lead to a reduced-order model with an a priori bound on the approximation error. For large scale problems, balanced truncation becomes inefficient and moment-matching methods, based on the construction of Krylov subspaces, are more appropriate [11, 12]. For linear mechanical systems, extensions of both approaches have been proposed in order to preserve the structure of the equations of motion [13, 14, 15].

In linear structural dynamics, component-mode techniques have been initially developed for substructuring applications. Exploiting the second-order and lightly damped nature of mechanical systems, a subspace of the configuration space is constructed by combination of various sets of modes (e.g. static modes, rigid modes, eigenmodes, etc.). Among existing approaches, the methods of Hurty [16], Craig and Bampton [17], Mac Neal [18] and Rubin [19] should be mentioned. We also refer to the review paper by Craig [20] and to the book of Géradin and Rixen [21].

In multibody dynamics, linear reduction techniques can be exploited for the efficient kinematic description of an *isolated flexible body* with respect to a floating frame of reference [1, 4, 6]. In order to obtain a more drastic reduction, we propose to define a reduction procedure for the *whole mechanism*, including all bodies and joints. Therefore, reduction techniques for constrained nonlinear systems should be considered.

1.2 Linear subspaces for nonlinear systems

The dynamics of a nonlinear system can still be projected onto a unique linear subspace. Here, we make the distinction between data-based and linearization-based methods.

On the one hand, data-based methods, such as the proper orthogonal decomposition [22] or the empirical balanced realization [23], make use of a set of data taken either from experiments or from numerical simulations, and consisting of sampled measurements (snapshots) of the state or of the configuration vector. Using a singular value analysis, a subspace is constructed in order to obtain the best approximation of the available data. Those methods are thus sensitive to the selected data, which is an important drawback. The reduced-order model is defined by projection of the initial model, and it is not available in closed-form.

On the other hand, at a given configuration, a linear reduction technique can be applied to the linearized equations of motion, leading to a reduced-order model with a local validity. A global reduced-order model might be obtained by combination of local models computed at several linearization points [24] (for consistency, the same subspace of projection should be used at all linearization points). In the theory of linear parameter varying systems [25, 26, 27, 28, 29], various weighting, approximation or interpolation techniques have been considered, and dedicated control schemes have been developed. However, for mechanical systems, the Lagrangian structure is hardly preserved by such linearization-based methods.

1.3 Submanifolds for nonlinear systems

Two additional difficulties are associated with linear projection techniques. First, the dimension of the subspace should be rather high in order to capture the nonlinear effects, and second, nonlinear constraints cannot be eliminated: they still appear in the reduced model.

Those facts motivate the investigation of nonlinear projection techniques. A projection onto a submanifold can be obtained in two steps: (i) a full nonlinear coordinate transformation into modal coordinates, (ii) a truncation of the modal basis. For the problem (i), Scherpen [30] has extended the concept of balancing to nonlinear ODE systems. However, to our knowledge, this approach has only been successfully applied to simple academic systems.

In order to develop a method applicable to realistic multibody systems with nonlinear holonomic constraints, the physical properties of the system can be exploited for the construction of an adequate nonlinear coordinate transformation. We call the resulting reduced parameterization the *Global Modal Parameterization (GMP)*.

1.4 Outline

For a general holonomic Lagrangian system, section 2 defines the general framework for a model reduction procedure, which accounts for the gyroscopic and centrifugal forces, and which preserves the Lagrangian structure. At this level, we assume the existence of a modal parameterization with independent coordinates.

Section 3 is dedicated to the construction of the GMP, based on a decomposition of the motion into a large amplitude rigid motion and a small amplitude elastic displacement. The order reduction follows from a parametric component-mode synthesis in the configuration space. The consistency and the validity of the GMP are analysed in detail. In particular, we show that a mode tracking strategy needs to be implemented in the configuration space.

Section 4 describes the reduced-order model and the numerical reduction algorithm. We consider that the initial model is formulated according to the nonlinear finite element method, but since our theory assumes linear elasticity, other initial formulations could have been selected. Even though the global consistency of the reduced-order model is guaranteed, the reduction algorithm only gives the numerical value of its parameters locally at a given configuration.

In order to build a closed-form expression in the configuration space, an approximation strategy is developed in section 5. As in rigid robotics, a simple look-up table technique could be considered (Raibert [31]), but we prefer a more advanced approach. For instance, artificial neural networks, kriging, polynomial or rational approximations can be used to solve this standard approximation problem. We present an adaptive piecewise polynomial approximation, which appears very effective for our applications.

Two examples are considered in section 6: a flexible four-bar mechanism and a large manipulator. For this last application, the reduced-order model has been used for control design and experimental results are reported. Finally, some conclusions are drawn in section 7.

2 LAGRANGIAN MECHANICS AND MODEL REDUCTION

2.1 Equations of motion for a constrained mechanical system

Let us consider a holonomic dynamic system, with a $n \times 1$ vector of generalized coordinates \mathbf{q} . For a flexible mechanism, those coordinates may be absolute nodal coordinates, Cartesian coordinates and/or relative coordinates. The system is characterized by

- its potential energy: $\mathcal{V}(\mathbf{q})$,
- its kinetic energy: $\mathcal{K}(\mathbf{q}, \dot{\mathbf{q}}) = \frac{1}{2} \dot{\mathbf{q}}^T \mathbf{M}^{\mathbf{q}\mathbf{q}}(\mathbf{q}) \dot{\mathbf{q}}$ ($\mathbf{M}^{\mathbf{q}\mathbf{q}}$ is the symmetric mass matrix),
- a set of m independent holonomic kinematic constraints: $\Phi(\mathbf{q}) = \mathbf{0}$,
- the virtual work of applied generalized forces $\mathbf{g}^{\mathbf{q}}$: $\delta\mathcal{W} = \delta\mathbf{q}^T \mathbf{g}^{\mathbf{q}}$.

The real trajectory between the time instants t_1 and t_2 satisfies the Hamilton principle. Following the Lagrange multiplier method, this principle is equivalent to:

$$\int_{t_1}^{t_2} [\delta(\mathcal{L} - \boldsymbol{\lambda}^T \Phi) + \delta\mathcal{W}] dt = 0$$

where $\mathcal{L} = \mathcal{K} - \mathcal{V}$ is the Lagrangian of the system and $\boldsymbol{\lambda}$ is the $m \times 1$ vector of Lagrange multipliers. If $\Phi_{,\mathbf{q}}$ denotes the constraint gradient, the resulting Lagrange equations of motion are:

$$\mathbf{M}^{\mathbf{q}\mathbf{q}} \ddot{\mathbf{q}} + \mathbf{h}^{\mathbf{q}}(\mathbf{q}, \dot{\mathbf{q}}) + \mathcal{V}_{,\mathbf{q}} + \Phi_{,\mathbf{q}}^T \boldsymbol{\lambda} = \mathbf{g}^{\mathbf{q}} \quad (1)$$

$$\Phi(\mathbf{q}) = \mathbf{0}$$

$\mathbf{h}^{\mathbf{q}}$ gathers the centrifugal and Coriolis inertia forces which are quadratic in $\dot{\mathbf{q}}$. Using the index summation convention, we have:

$$(h^{\mathbf{q}})_i = (\Gamma^{qqq})_{ijk} \dot{q}_j \dot{q}_k$$

where $(\Gamma^{qqq})_{ijk}$ is the Christoffel symbol of the first kind:

$$(\Gamma^{qqq})_{ijk} = \frac{1}{2} \left(\frac{\partial(M^{qq})_{ij}}{\partial q_k} + \frac{\partial(M^{qq})_{ik}}{\partial q_j} - \frac{\partial(M^{qq})_{jk}}{\partial q_i} \right) \quad \text{and} \quad (\Gamma^{qqq})_{ijk} = (\Gamma^{qqq})_{ikj} \quad (2)$$

Example: Rotating rigid body

In order to illustrate the connection between the Christoffel symbol and classical multibody formalisms, we consider the rotation kinetic energy of a rigid body about its center of gravity:

$$\mathcal{K} = \frac{1}{2} \boldsymbol{\Omega}^T \mathbf{J}^{\boldsymbol{\Omega}\boldsymbol{\Omega}} \boldsymbol{\Omega}$$

$\mathbf{J}^{\boldsymbol{\Omega}\boldsymbol{\Omega}}$ is the constant inertia tensor, and $\boldsymbol{\Omega}$ is the 3×1 vector of material angular velocities. The motion can be parameterized using the Cartesian rotation vector $\boldsymbol{\alpha}$ [1], and the tangent operator $\mathbf{T}(\boldsymbol{\alpha})$ is such that $\boldsymbol{\Omega} = \mathbf{T}(\boldsymbol{\alpha}) \dot{\boldsymbol{\alpha}}$. The kinetic energy becomes:

$$\mathcal{K} = \frac{1}{2} \dot{\boldsymbol{\alpha}}^T \mathbf{M}^{\boldsymbol{\alpha}\boldsymbol{\alpha}} \dot{\boldsymbol{\alpha}} \quad \text{with} \quad \mathbf{M}^{\boldsymbol{\alpha}\boldsymbol{\alpha}} = \mathbf{T}^T \mathbf{J}^{\boldsymbol{\Omega}\boldsymbol{\Omega}} \mathbf{T}$$

For $\boldsymbol{\alpha} = \mathbf{0}$, \mathbf{T} is characterized by:

$$T_{ij} = (\delta^K)_{ij} \quad \text{and} \quad \frac{\partial T_{ij}}{\partial \alpha_k} = \frac{1}{2} \epsilon_{ijk}$$

where $(\delta^K)_{ij}$ is the Kronecker symbol, and ϵ_{ijk} is the alternating symbol, which is equal to 1 if (ijk) is a cyclic permutation of (123) , to -1 if (ijk) is an anticyclic permutation of (123) , and to 0 otherwise. According to (2), the Christoffel symbol is then:

$$(\Gamma^{\alpha\alpha\alpha})_{ijk} = \frac{1}{2} [\epsilon_{uik} (J^{\Omega\Omega})_{uj} + \epsilon_{uij} (J^{\Omega\Omega})_{uk}]$$

2.2 Problem statement

Usually, the control engineer is only interested in the response of $n^o < n$ output dofs \mathbf{q}^o , when actuator or disturbance forces \mathbf{g}^v are applied to $n^v < n$ input dofs. We have the relations:

$$\mathbf{q}^o = \mathbf{L}^{oq} \mathbf{q}, \quad \mathbf{g}^q = (\mathbf{L}^{vq})^T \mathbf{g}^v \quad (3)$$

where \mathbf{L}^{oq} and \mathbf{L}^{vq} are boolean localization matrices. In many practical cases, the sets of input and output dofs are equivalent: $\mathbf{L}^{oq} = \mathbf{L}^{vq}$, and it is more relevant to talk about interface dofs. For given initial conditions, the model of the dynamic system defined by (1) and (3) can be considered as an operator $\widehat{\Sigma}$, which maps the input signals $\mathbf{g}^v(t)$ to the outputs $\mathbf{q}^o(t)$:

$$\mathbf{q}^o(t) = \widehat{\Sigma}(\mathbf{g}^v(t))$$

The objective of a model reduction technique is to derive a simpler approximation Σ of the initial model $\widehat{\Sigma}$. More precisely, for control applications, the reduced model Σ should be more appropriate in the sense defined at the beginning of our introduction. The next section shows that such a reduced-model can be obtained by a nonlinear projection.

2.3 Nonlinear reduction by projection

In a first step, we would like to eliminate the constraints and to get rid of the Lagrange multipliers. This can be realized if a parameterization with $n - m$ independent modal coordinates $\widehat{\boldsymbol{\eta}}$ is available. The coordinate transformation

$$\mathbf{q} = \mathbf{q}(\widehat{\boldsymbol{\eta}}) \quad (4)$$

should be invertible, sufficiently continuous, and consistent with the constraints:

$$\Phi(\mathbf{q}(\widehat{\boldsymbol{\eta}})) = \mathbf{0}, \quad \forall \widehat{\boldsymbol{\eta}} \quad (5)$$

In a second step, a partitioning into n^η dominant modes $\boldsymbol{\eta}$ and n^ϵ higher-order modes $\boldsymbol{\eta}^\epsilon$ is considered:

$$\widehat{\boldsymbol{\eta}} = \begin{bmatrix} \boldsymbol{\eta} \\ \boldsymbol{\eta}^\epsilon \end{bmatrix}$$

and the order reduction follows from a projection of the initial model onto the subspace $\boldsymbol{\eta}^\epsilon = \mathbf{0}$. Indeed, in this subspace, the coordinate transformation (4) is restated as

$$\mathbf{q} = \mathbf{q}(\boldsymbol{\eta})$$

Introducing this transformation into the expression of the potential energy, of the external work and of the kinetic energy, we obtain the Lagrange equations for the reduced-order model:

$$\mathbf{M}^{\eta\eta} \ddot{\boldsymbol{\eta}} + \mathbf{h}^\eta(\boldsymbol{\eta}, \dot{\boldsymbol{\eta}}) + \mathcal{V}_{,\eta} = \mathbf{g}^\eta \quad (6)$$

with:

$$\mathcal{V}_{,\eta} = \mathbf{q}_{,\eta}^T \mathcal{V}_{,\mathbf{q}} \quad (7)$$

$$\mathbf{g}^\eta = \mathbf{q}_{,\eta}^T \mathbf{g}^\mathbf{q} \quad (8)$$

$$\mathbf{M}^{\eta\eta} = \mathbf{q}_{,\eta}^T \mathbf{M}^{\mathbf{q}\mathbf{q}} \mathbf{q}_{,\eta} \quad (9)$$

$$(h^\eta)_i = (\Gamma^{\eta\eta\eta})_{ijk} (\dot{\eta})_j (\dot{\eta})_k \quad (10)$$

The components of the new Christoffel symbol $(\Gamma^{\eta\eta\eta})_{ijk}$ are easily obtained from (2) and (9):

$$(\Gamma^{\eta\eta\eta})_{ijk} = \frac{\partial q_u}{\partial \eta_i} \frac{\partial q_v}{\partial \eta_j} \frac{\partial q_w}{\partial \eta_k} (\Gamma^{qqq})_{uvw} + \frac{\partial q_u}{\partial \eta_i} \frac{\partial^2 q_v}{\partial \eta_j \partial \eta_k} (M^{qq})_{uv} \quad (11)$$

In equations (10) and (11), indices i, j, k are in the range $1, \dots, n^\eta$, while indices u, v, w are in the range $1, \dots, n$. It is noticeable that the transformation (11) involves not only the Jacobian of the coordinate transformation but also the second-order derivatives or curvatures, which reflects the non-tensorial nature of the Christoffel symbol [32]. Clearly, the contribution of the curvatures would vanish for a linear coordinate transformation.

The quality of the approximation Σ depends on the ability of the dominant modes $\boldsymbol{\eta}$ to capture the essential dynamics of the initial model. In multibody dynamics, the distinction between rigid and flexible modes is essential for the definition of an effective Global Modal Parameterization.

3 THE GLOBAL MODAL PARAMETERIZATION

Before defining the GMP, the concepts of rigid and flexible configuration spaces should be clarified. For a flexible mechanism with s rigid kinematic modes, we have the inequality:

$$s \leq n - m$$

and the particular case $s = n - m$ corresponds to a rigid mechanism. The *flexible manifold* $\widehat{\Omega}_{\mathbf{q}}^{ft}$, with intrinsic dimension $n - m$, is defined as the set of kinematically admissible configurations which satisfy the m kinematic constraints:

$$\widehat{\Omega}_{\mathbf{q}}^{ft} = \{\mathbf{q} \in \mathcal{R}^n \mid \Phi(\mathbf{q}) = \mathbf{0}\}$$

In contrast, the *rigid configuration space* $\Omega_{\mathbf{q}}^{rt} \subset \widehat{\Omega}_{\mathbf{q}}^{ft}$, with intrinsic dimension s , is defined as the set of undeformed configurations. The motivation for the notations $\widehat{\Omega}_{\mathbf{q}}^{ft}$ and $\Omega_{\mathbf{q}}^{rt}$ will become clearer in the following (the superscript t stands for “total”).

3.1 Definition of the GMP

A few physical considerations and assumptions lead to the definition of the GMP.

1. The overall motion is decomposed into a large amplitude rigid motion $\mathbf{q}^r \in \Omega_{\mathbf{q}}^{rt}$ and a small amplitude elastic displacement \mathbf{q}^f :

$$\mathbf{q} = \mathbf{q}^r + \mathbf{q}^f$$

2. As will be discussed in section 3.2, a restricted part of the rigid configuration space $\Omega_{\mathbf{q}}^r \subset \Omega_{\mathbf{q}}^{rt}$ can be parameterized using s independent parameters $\boldsymbol{\theta}$. Hence, there exists a regular and invertible kinematic mapping $\boldsymbol{\rho}$:

$$\boldsymbol{\rho} : \Omega_{\boldsymbol{\theta}} \rightarrow \Omega_{\mathbf{q}}^r, \quad \boldsymbol{\theta} \mapsto \mathbf{q}^r = \boldsymbol{\rho}(\boldsymbol{\theta})$$

where $\Omega_{\boldsymbol{\theta}} \subset \mathcal{R}^s$ represents the set of allowed variations of $\boldsymbol{\theta}$.

3. The elastic displacement is a deviation from the rigid motion, which is parameterized using $(n - m) - s$ independent modal coordinates $\widehat{\boldsymbol{\delta}}$:

$$\mathbf{q}^f = \mathbf{q}^f(\boldsymbol{\theta}, \widehat{\boldsymbol{\delta}}) \quad \text{with} \quad \mathbf{q}^f(\boldsymbol{\theta}, \mathbf{0}) = \mathbf{0}, \quad \forall \boldsymbol{\theta} \in \Omega_{\boldsymbol{\theta}} \quad (12)$$

Under the small deformation assumption, we make a first-order MacLaurin expansion with respect to $\widehat{\boldsymbol{\delta}}$:

$$\mathbf{q}^f(\boldsymbol{\theta}, \widehat{\boldsymbol{\delta}}) \simeq \frac{\partial \mathbf{q}^f}{\partial \widehat{\boldsymbol{\delta}}}(\boldsymbol{\theta}, \mathbf{0}) \widehat{\boldsymbol{\delta}} = \boldsymbol{\Psi}^{\mathbf{q}\widehat{\boldsymbol{\delta}}}(\boldsymbol{\theta}) \widehat{\boldsymbol{\delta}}$$

$\partial \mathbf{q}^f / \partial \widehat{\boldsymbol{\delta}}$ is interpreted as a flexible mode shape matrix $\boldsymbol{\Psi}^{\mathbf{q}\widehat{\boldsymbol{\delta}}}$, which depends on the configuration $\boldsymbol{\theta}$. In section 3.3, we shall see that $\boldsymbol{\Psi}^{\mathbf{q}\widehat{\boldsymbol{\delta}}}(\boldsymbol{\theta})$ can be constructed according to a parametric component-mode synthesis in $\Omega_{\boldsymbol{\theta}}$.

4. Considering a partitioning of the flexible modes into n^{δ} dominant modes $\boldsymbol{\delta}$ and n^{ϵ} higher-order modes $\boldsymbol{\delta}^{\epsilon}$:

$$\widehat{\boldsymbol{\delta}} = \begin{bmatrix} \boldsymbol{\delta} \\ \boldsymbol{\delta}^{\epsilon} \end{bmatrix}, \quad \mathbf{q}^f = \boldsymbol{\Psi}^{\mathbf{q}\boldsymbol{\delta}}(\boldsymbol{\theta}) \boldsymbol{\delta} + \boldsymbol{\Psi}^{\mathbf{q}\boldsymbol{\delta}^{\epsilon}}(\boldsymbol{\theta}) \boldsymbol{\delta}^{\epsilon}$$

the order reduction is obtained by a projection onto the subspace $\boldsymbol{\delta}^{\epsilon} = \mathbf{0}$. In this subspace, we have:

$$\mathbf{q}^f = \boldsymbol{\Psi}^{\mathbf{q}\boldsymbol{\delta}}(\boldsymbol{\theta}) \boldsymbol{\delta}$$

In summary, the Global Modal Parameterization is a mapping

$$\boxed{\text{GMP} : \Omega_{\boldsymbol{\theta}} \times \Omega_{\boldsymbol{\delta}} \rightarrow \Omega_{\mathbf{q}}^f, \quad (\boldsymbol{\theta}, \boldsymbol{\delta}) \mapsto \mathbf{q} = \boldsymbol{\rho}(\boldsymbol{\theta}) + \boldsymbol{\Psi}^{\mathbf{q}\boldsymbol{\delta}}(\boldsymbol{\theta}) \boldsymbol{\delta}} \quad (13)$$

whose regularity and invertibility will be demonstrated in section 3.4. $\Omega_{\boldsymbol{\delta}} \subset \mathcal{R}^{n^{\delta}}$ represents the set of allowed variations of $\boldsymbol{\delta}$ (it is a neighbourhood of the origin), and $\Omega_{\mathbf{q}}^f \subset \widehat{\Omega}_{\mathbf{q}}^{ft}$ is a submanifold of the flexible manifold. To make a connection with section 2.3, we have:

$$\widehat{\boldsymbol{\eta}} = \begin{bmatrix} \boldsymbol{\theta} \\ \widehat{\boldsymbol{\delta}} \end{bmatrix} \quad \text{and} \quad \boldsymbol{\eta} = \begin{bmatrix} \boldsymbol{\theta} \\ \boldsymbol{\delta} \end{bmatrix}$$

The reduction formulae (7) to (11) require the first and second-order derivatives of the coordinate transformation. The differentiation of the GMP and the interpretation of the Jacobian $\boldsymbol{\rho}_{,\boldsymbol{\theta}}(\boldsymbol{\theta})$ as a matrix of rigid-body modes $\boldsymbol{\Psi}^{\mathbf{q}\boldsymbol{\theta}}(\boldsymbol{\theta})$ lead to:

$$\mathbf{q}_{,\boldsymbol{\eta}}(\boldsymbol{\theta}, \boldsymbol{\delta}) = \begin{bmatrix} \boldsymbol{\Psi}^{\mathbf{q}\boldsymbol{\theta}}(\boldsymbol{\theta}) + \frac{\partial}{\partial \boldsymbol{\theta}} (\boldsymbol{\Psi}^{\mathbf{q}\boldsymbol{\delta}}(\boldsymbol{\theta}) \boldsymbol{\delta}) & \boldsymbol{\Psi}^{\mathbf{q}\boldsymbol{\delta}}(\boldsymbol{\theta}) \end{bmatrix} \quad (14)$$

so that for an undeformed configuration ($\boldsymbol{\delta} = \mathbf{0}$):

$$\mathbf{q}_{,\boldsymbol{\eta}}(\boldsymbol{\theta}, \mathbf{0}) = [\boldsymbol{\Psi}^{\mathbf{q}\boldsymbol{\theta}}(\boldsymbol{\theta}) \quad \boldsymbol{\Psi}^{\mathbf{q}\boldsymbol{\delta}}(\boldsymbol{\theta})] = \boldsymbol{\Psi}^{\mathbf{q}\boldsymbol{\eta}}(\boldsymbol{\theta}) \quad (15)$$

At an undeformed configuration, the second-order derivatives are associated with the sensitivities of the rigid and flexible modes:

$$\frac{\partial^2 q_i}{\partial \theta_j \partial \theta_k}(\boldsymbol{\theta}, \mathbf{0}) = \frac{\partial (\boldsymbol{\Psi}^{\mathbf{q}\boldsymbol{\theta}})_{ik}}{\partial \theta_j}, \quad \frac{\partial^2 q_i}{\partial \theta_j \partial \delta_k}(\boldsymbol{\theta}, \mathbf{0}) = \frac{\partial (\boldsymbol{\Psi}^{\mathbf{q}\boldsymbol{\delta}})_{ik}}{\partial \theta_j}, \quad \frac{\partial^2 q_i}{\partial \delta_j \partial \delta_k}(\boldsymbol{\theta}, \mathbf{0}) = 0 \quad (16)$$

In order to exploit the Lagrange multiplier technique, the GMP should be formulated in terms of the augmented coordinates \mathbf{u} :

$$\mathbf{u} = \begin{bmatrix} \mathbf{q} \\ \boldsymbol{\lambda} \end{bmatrix}$$

The Lagrange multipliers represent internal forces and, in the absence of external loads, their value is zero at an undeformed configuration. Assuming linear elasticity, $\boldsymbol{\lambda}$ is proportional to $\boldsymbol{\delta}$, and the GMP is reformulated:

$$\text{GMP}^{\mathbf{u}} : \Omega_{\boldsymbol{\theta}} \times \Omega_{\boldsymbol{\delta}} \rightarrow \Omega_{\mathbf{u}}^f, \quad (\boldsymbol{\theta}, \boldsymbol{\delta}) \mapsto \begin{bmatrix} \mathbf{q} \\ \boldsymbol{\lambda} \end{bmatrix} = \begin{bmatrix} \boldsymbol{\rho}(\boldsymbol{\theta}) \\ \mathbf{0} \end{bmatrix} + \begin{bmatrix} \boldsymbol{\Psi}^{\mathbf{q}\boldsymbol{\delta}}(\boldsymbol{\theta}) \\ \boldsymbol{\Psi}^{\boldsymbol{\lambda}\boldsymbol{\delta}}(\boldsymbol{\theta}) \end{bmatrix} \boldsymbol{\delta}$$

with $\Omega_{\mathbf{u}}^f \subset \Omega_{\mathbf{q}}^f \times \mathcal{R}^m$. We shall use the equivalent notations:

$$\text{GMP}^{\mathbf{u}} : \Omega_{\boldsymbol{\theta}} \times \Omega_{\boldsymbol{\delta}} \rightarrow \Omega_{\mathbf{u}}^f, \quad (\boldsymbol{\theta}, \boldsymbol{\delta}) \mapsto \mathbf{u} = \boldsymbol{\rho}^{\mathbf{u}}(\boldsymbol{\theta}) + \boldsymbol{\Psi}^{\mathbf{u}\boldsymbol{\delta}}(\boldsymbol{\theta}) \boldsymbol{\delta}$$

Moreover, the augmented rigid configuration spaces are trivially defined by:

$$\Omega_{\mathbf{u}}^{rt} = \Omega_{\mathbf{q}}^{rt} \times \{0\}^m, \quad \Omega_{\mathbf{u}}^r = \Omega_{\mathbf{q}}^r \times \{0\}^m$$

The next two sections give more details about the parameterization of the rigid motion and of the flexible motion, respectively. Afterwards, section 3.4 will demonstrate the consistency of the GMP.

3.2 Parameterization of the rigid kinematics

We seek for a set of s independent coordinates $\boldsymbol{\theta}$ able to parameterize the rigid configuration space $\Omega_{\mathbf{u}}^{rt}$. For parallel kinematic machines, $\Omega_{\mathbf{u}}^{rt}$ is a manifold which cannot be globally parameterized using a unique set of independent coordinates. In other words, any set of minimal coordinates leads to singular configurations, which represent bounds for the validity of the parameterization. We refer to [33, 34, 35, 36] for detailed analysis of singularities in mechanism analysis. Our objective is to define a minimal parameterization with a relevant validity region $\Omega_{\mathbf{u}}^r \subset \Omega_{\mathbf{u}}^{rt}$.

We propose to select the minimal coordinates $\boldsymbol{\theta}$ as the *actuated coordinates*, i.e. the coordinates associated with the generalized forces exerted by the actuators. For instance, for a motorized hinge, the actuated coordinate is the angle between the connected links, whereas for a linear actuator, it is the relative distance between the connected bodies. As a consequence of this choice, the actuator coordinates will appear explicitly in the reduced model, which is extremely valuable for the design of the control system. An implicit assumption is that the number of actuators is equal to s . This does not imply that the reduction method is only applicable to fully actuated mechanisms, it simply means that in any other situation, the definition of the independent parameters is left to the user.

Thus, our parameterization is only valid in a region $\Omega_{\mathbf{u}}^r \subset \Omega_{\mathbf{u}}^{rt}$ which is free from actuator singularities, as illustrated in Figure 1. This is not really restrictive since, for most applications, actuator singularities are also carefully avoided for controllability reasons (at those configurations, the mechanism could move even though all actuators were blocked).

$\Omega_{\boldsymbol{\theta}} \subset \mathcal{R}^s$ represents the corresponding set of allowed actuator motions. For a given $\boldsymbol{\theta} \in \Omega_{\boldsymbol{\theta}}$, the vector $\mathbf{u} = \boldsymbol{\rho}^{\mathbf{u}}(\boldsymbol{\theta})$ can be computed according to a standard zero-strain analysis, which is described in [36], and summarized hereafter. First of all, we consider that the actuator coordinates are included among the set of n coordinates \mathbf{q} , so that:

$$\mathbf{u} = \begin{bmatrix} \boldsymbol{\theta} \\ \mathbf{q}^* \\ \boldsymbol{\lambda} \end{bmatrix} = \begin{bmatrix} \boldsymbol{\theta} \\ \mathbf{u}^* \end{bmatrix}$$

where \mathbf{q}^* are the $n - s$ non-actuated coordinates. Any static equilibrium configuration achieves a minimum of the augmented elastic potential energy $\mathcal{V} + \boldsymbol{\lambda}^T \boldsymbol{\Phi}$, which leads to the stationarity conditions:

$$\begin{aligned} \mathcal{V}_{,\mathbf{q}^*} + \boldsymbol{\Phi}_{,\mathbf{q}^*}^T \boldsymbol{\lambda} &= \mathbf{0} \\ \boldsymbol{\Phi}_{,\mathbf{q}} &= \mathbf{0} \end{aligned} \tag{17}$$

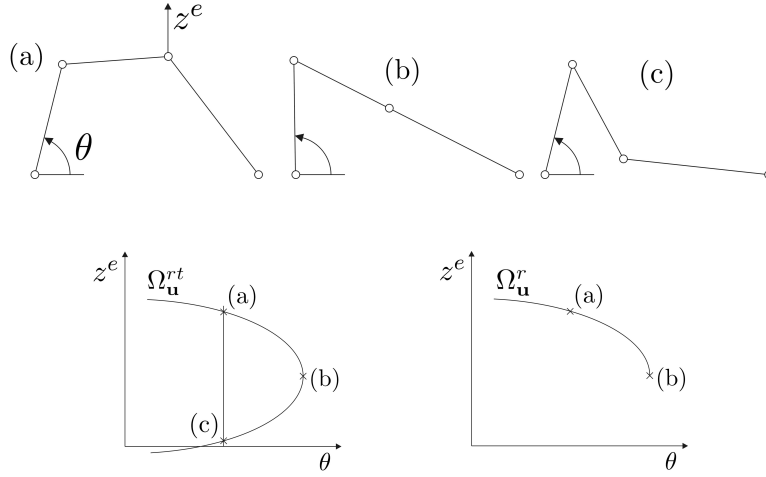


Figure 1: Rigid four bar mechanism, with an actuator at the lower left hinge. The configuration space is a 1-dimensional manifold, whose projection in the plane of the coordinates z^e and θ is also represented. Configuration (b) is an actuator singularity; it separates two regions for which the actuator parameterization is regular. The parameterization is not regular in the total configuration space $\Omega_{\mathbf{u}}^{rt}$, since configurations (a) and (c) are possible for the same value of θ .

Starting from a known reference configuration $\mathbf{u}_{ref} = \boldsymbol{\rho}^{\mathbf{u}}(\boldsymbol{\theta}_{ref})$, and given a target value $\boldsymbol{\theta} \in \Omega_{\boldsymbol{\theta}}$, this nonlinear equation can be solved for \mathbf{u}^* according to a Newton procedure. If the reference and the target configurations are sufficiently close to each other, the algorithm converges to the unique solution $\mathbf{u} \in \Omega_{\mathbf{u}}^r$. Otherwise, intermediate configurations have to be considered, so that the algorithm can progress sequentially to the target configuration with several smaller increments.

For pre-stressed mechanisms, the concept of rigid configuration space should be replaced by the concept of “equilibrium configuration space”. Equation (17) would still be relevant, but the internal forces $\boldsymbol{\lambda}$ and the actuator forces $\mathcal{V}_{,\boldsymbol{\theta}}$ might be different from zero at a static equilibrium. In this paper, we do not want to enter into more details, and we leave the problem of pre-stressed mechanisms aside.

3.3 Parameterization of the flexible motion

The Global Modal Parameterization (GMP) involves a configuration-dependent mode-shape matrix $\boldsymbol{\Psi}^{\mathbf{u}\delta}(\boldsymbol{\theta})$, which is defined by a parametric component-mode synthesis. Indeed, given a configuration $\boldsymbol{\theta} \in \Omega_{\boldsymbol{\theta}}$, the mode-shape matrix $\boldsymbol{\Psi}^{\mathbf{u}\delta}$ is constructed as an optimal basis to describe the *linearized motion* around the state $\mathbf{q} = \boldsymbol{\rho}(\boldsymbol{\theta})$, $\dot{\mathbf{q}} = \mathbf{0}$:

$$\begin{bmatrix} \mathbf{M}^{\mathbf{q}\mathbf{q}} & \mathbf{0} \\ \mathbf{0} & \mathbf{0} \end{bmatrix} \begin{bmatrix} \Delta \ddot{\mathbf{q}} \\ \Delta \ddot{\boldsymbol{\lambda}} \end{bmatrix} + \begin{bmatrix} \mathbf{K}_t^{\mathbf{q}\mathbf{q}} & \boldsymbol{\Phi}_{,\mathbf{q}}^T \\ \boldsymbol{\Phi}_{,\mathbf{q}} & \mathbf{0} \end{bmatrix} \begin{bmatrix} \Delta \mathbf{q} \\ \Delta \boldsymbol{\lambda} \end{bmatrix} = \begin{bmatrix} \mathbf{0} \\ \mathbf{0} \end{bmatrix} \quad (18)$$

$\mathbf{K}_t^{\mathbf{q}\mathbf{q}}$ is the exact tangent stiffness operator, whose expression is detailed in [36].

We consider a partitioning of the $n + m$ initial dofs:

$$\mathbf{u} = \begin{bmatrix} \boldsymbol{\theta} \\ \mathbf{q}^{\mathbf{g}} \\ \mathbf{u}^{\mathbf{i}} \end{bmatrix}$$

$\boldsymbol{\theta}$ are s actuator (or rigid) dofs, $\mathbf{q}^{\mathbf{g}}$ are $n^{\mathbf{g}}$ constraint dofs where additional external loads are applied, and $\mathbf{u}^{\mathbf{i}}$ are the remaining internal dofs, including the Lagrange multipliers, which

are not loaded and can be condensed by the reduction procedure. Accordingly, the mass and stiffness matrices appearing in (18) are rewritten:

$$\begin{bmatrix} \mathbf{M}^{\text{rr}} & \mathbf{M}^{\text{rg}} & \mathbf{M}^{\text{ri}} \\ \mathbf{M}^{\text{gr}} & \mathbf{M}^{\text{gg}} & \mathbf{M}^{\text{gi}} \\ \mathbf{M}^{\text{ir}} & \mathbf{M}^{\text{ig}} & \mathbf{M}^{\text{ii}} \end{bmatrix}, \quad \begin{bmatrix} \mathbf{K}^{\text{rr}} & \mathbf{K}^{\text{rg}} & \mathbf{K}^{\text{ri}} \\ \mathbf{K}^{\text{gr}} & \mathbf{K}^{\text{gg}} & \mathbf{K}^{\text{gi}} \\ \mathbf{K}^{\text{ir}} & \mathbf{K}^{\text{ig}} & \mathbf{K}^{\text{ii}} \end{bmatrix}$$

and a complete basis of modes is defined:

- The s rigid modes $\Psi^{\text{u}\theta}$, which also form the Jacobian of $\rho^{\text{u}}(\theta)$, satisfy:

$$\begin{bmatrix} \mathbf{K}^{\text{rr}} & \mathbf{K}^{\text{rg}} & \mathbf{K}^{\text{ri}} \\ \mathbf{K}^{\text{gr}} & \mathbf{K}^{\text{gg}} & \mathbf{K}^{\text{gi}} \\ \mathbf{K}^{\text{ir}} & \mathbf{K}^{\text{ig}} & \mathbf{K}^{\text{ii}} \end{bmatrix} \begin{bmatrix} \mathbf{I} \\ \Psi^{\text{g}\theta} \\ \Psi^{\text{i}\theta} \end{bmatrix} = \begin{bmatrix} \mathbf{0} \\ \mathbf{0} \\ \mathbf{0} \end{bmatrix}, \quad \Psi^{\text{u}\theta} = \begin{bmatrix} \mathbf{I} \\ \Psi^{\text{g}\theta} \\ \Psi^{\text{i}\theta} \end{bmatrix}$$

- The n^{g} constraint modes $\Psi^{\text{u}\gamma}$ are the static deformations obtained when the rigid dofs θ are fixed and unit displacements are imposed to the constrained dofs \mathbf{q}^{g} :

$$\begin{bmatrix} \mathbf{K}^{\text{gg}} & \mathbf{K}^{\text{gi}} \\ \mathbf{K}^{\text{ig}} & \mathbf{K}^{\text{ii}} \end{bmatrix} \begin{bmatrix} \mathbf{I} \\ \Psi^{\text{i}\gamma} \end{bmatrix} = \begin{bmatrix} \mathbf{g}^{\text{g}} \\ \mathbf{0} \end{bmatrix}, \quad \Psi^{\text{u}\gamma} = \begin{bmatrix} \mathbf{0} \\ \mathbf{I} \\ \Psi^{\text{i}\gamma} \end{bmatrix} \quad (19)$$

- The internal modes $\Psi^{\text{u}\hat{\omega}}$ are the normalized eigenmodes when rigid and constraint dofs are fixed. Each eigenmode $\Psi^{\text{u}k}$ is one solution to the eigenvalue problem:

$$(\mathbf{K}^{\text{ii}} - \omega_k^2 \mathbf{M}^{\text{ii}}) \Psi^{\text{ik}} = \mathbf{0}, \quad (\Psi^{\text{ik}})^T \mathbf{M}^{\text{ii}} \Psi^{\text{ik}} = 1, \quad \Psi^{\text{u}k} = \begin{bmatrix} \mathbf{0} \\ \mathbf{0} \\ \Psi^{\text{ik}} \end{bmatrix} \quad (20)$$

If the modes are sorted by eigenvalue, $\Psi^{\text{u}\hat{\omega}}$ can be partitioned into n^{t} dominant modes $\Psi^{\text{u}\omega}$ and n^{e} higher-order modes $\Psi^{\text{u}\epsilon}$:

$$\Psi^{\text{u}\hat{\omega}} = [\Psi^{\text{u}\omega} \quad \Psi^{\text{u}\epsilon}]$$

The total matrix of flexible modes is:

$$\Psi^{\text{u}\hat{\delta}} = [\Psi^{\text{u}\gamma} \quad \Psi^{\text{u}\omega} \quad \Psi^{\text{u}\epsilon}]$$

The reduction method of Hurty [16] relies on a truncation of the higher-order modes:

$$\Psi^{\text{u}\delta} = [\Psi^{\text{u}\gamma} \quad \Psi^{\text{u}\omega}], \quad n^{\delta} = n^{\text{g}} + n^{\text{t}}$$

This leads to an exact representation of the static response of the structure at the interface dofs (θ and \mathbf{q}^{g}). The method of Craig and Bampton [17], which does not isolate the rigid modes from the flexible modes, is clearly irrelevant in this context.

3.4 Consistency of the Global Modal Parameterization

The GMP (13) is a regular coordinate transformation if the following criteria are satisfied:

- It defines a bijection between $\Omega_{\theta} \times \Omega_{\delta}$ and $\Omega_{\mathbf{u}}^f$. This will be analysed in section 3.4.2.
- It is continuously differentiable in $\Omega_{\theta} \times \Omega_{\delta}$. By construction, the rigid mapping $\rho^{\text{u}}(\theta)$ is a smooth function in Ω_{θ} . In contrast, the flexible modes $\Psi^{\text{u}\delta}(\theta)$ have only been defined locally by component-mode synthesis, and their continuity will be analysed in sections 3.4.3 and 3.4.4.
- The Jacobian (14) has maximal rank in $\Omega_{\theta} \times \Omega_{\delta}$. This condition is easily checked: at an undeformed configuration, the Jacobian is composed of rigid and flexible modes, whose linear independence is guaranteed by construction. For small deformations, this property is preserved by continuity.

Moreover, we have to demonstrate that the constraints are automatically satisfied by the GMP (see condition (5)).

3.4.1 Satisfaction of the constraints

Let us introduce the GMP into the constraint equation and make a Taylor series expansion around an undeformed configuration:

$$\Phi(\rho(\theta) + \Psi^{\mathbf{q}\delta} \delta) = \Phi(\rho(\theta)) + \Phi_{,\mathbf{q}} \Psi^{\mathbf{q}\delta} \delta + \mathcal{O}(\|\delta\|^2)$$

The first term vanishes by definition of the rigid parameterization and the second by construction of the flexible modes (consider equations (19) and (20), and the structure of the stiffness matrix in (18)). As a conclusion, the constraints are automatically satisfied provided that second-order contributions of the deformations are negligible.

3.4.2 One-to-one property

To each vector $(\theta, \delta) \in \Omega_\theta \times \Omega_\delta$, the GMP assigns a unique vector $\mathbf{u} \in \Omega_{\mathbf{u}}^f$. This section demonstrates the converse: for a given $\mathbf{u} \in \Omega_{\mathbf{u}}^f$, there is only one $(\theta, \delta) \in \Omega_\theta \times \Omega_\delta$ such that $\mathbf{u} = \rho^{\mathbf{u}}(\theta) + \Psi^{\mathbf{u}\delta}(\theta) \delta$.

Suppose that another solution (θ', δ') also satisfies $\mathbf{u} = \rho^{\mathbf{u}}(\theta') + \Psi^{\mathbf{u}\delta'}(\theta') \delta'$. Since θ appears explicitly among the coordinates \mathbf{u} , we have $\theta' = \theta$, and the flexible coordinates satisfy:

$$\rho^{\mathbf{u}}(\theta) + \Psi^{\mathbf{u}\delta}(\theta) \delta = \rho^{\mathbf{u}}(\theta) + \Psi^{\mathbf{u}\delta'}(\theta) \delta' \quad \Rightarrow \quad \Psi^{\mathbf{u}\delta}(\theta) (\delta - \delta') = \mathbf{0}$$

From the linear independence of the flexible modes, we deduce that $\delta - \delta' = \mathbf{0}$.

3.4.3 Continuity of the constraint modes

The constraint modes $\Psi^{\mathbf{u}\gamma}$ are defined from a linear static analysis when the rigid dofs are fixed. From equation (19), we have

$$\Psi^{\mathbf{i}\gamma}(\theta) = -(\mathbf{K}^{\mathbf{ii}}(\theta))^{-1} \mathbf{K}^{\mathbf{ig}}(\theta)$$

Since $\mathbf{K}^{\mathbf{ii}}$ is invertible (otherwise additional rigid modes should be defined), and since every stiffness coefficient is continuous and differentiable, so are the constraint modes.

3.4.4 Continuity of the internal modes

The internal modes $\Psi^{\mathbf{i}u}$ are obtained after two steps: (i) the eigenvalue problem (20) is solved, (ii) the eigenmodes are sorted according to their eigenvalue, and the first n^t modes are selected.

For a simple eigenvalue ω_k and the associated internal mode ψ_k , it is instructive to differentiate the eigenvalue problem in (20). An infinitesimal variation $\Delta\theta_l$ of the coordinate θ_l leads to variations $\Delta\omega_k^2$ and $\Delta\psi_k$ such that:

$$\left(\frac{\partial \mathbf{K}^{\mathbf{ii}}}{\partial \theta_l} - \omega_k^2 \frac{\partial \mathbf{M}^{\mathbf{ii}}}{\partial \theta_l} \right) \psi_k \Delta\theta_l - \mathbf{M}^{\mathbf{ii}} \psi_k \Delta\omega_k^2 + (\mathbf{K}^{\mathbf{ii}} - \omega_k^2 \mathbf{M}^{\mathbf{ii}}) \Delta\psi_k = \mathbf{0} \quad (21)$$

A pre-multiplication by ψ_k^T together with the normalization condition in (20) yields:

$$\frac{\Delta\omega_k^2}{\Delta\theta_l} = \psi_k^T \left(\frac{\partial \mathbf{K}^{\mathbf{ii}}}{\partial \theta_l} - \omega_k^2 \frac{\partial \mathbf{M}^{\mathbf{ii}}}{\partial \theta_l} \right) \psi_k$$

Since the right-hand-side is well-defined, we conclude that the variations of ω_k^2 with respect to θ_l are continuous, and that the derivative $\partial\omega_k^2/\partial\theta_l$ exists (the continuity of the derivative

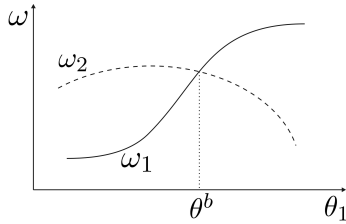


Figure 2: Crossing of the eigenfrequencies in a one-dimensional configuration space.

depends on the continuity of ψ_k). Thus, (21) can be rewritten:

$$(\mathbf{K}^{\text{ii}} - \omega_k^2 \mathbf{M}^{\text{ii}}) \frac{\Delta \psi_k}{\Delta \theta_l} = - \left(\frac{\partial \mathbf{K}^{\text{ii}}}{\partial \theta_l} - \omega_k^2 \frac{\partial \mathbf{M}^{\text{ii}}}{\partial \theta_l} - \frac{\partial \omega_k^2}{\partial \theta_l} \mathbf{M}^{\text{ii}} \right) \psi_k$$

Even though the right-hand-side is well-defined, $\Delta \psi_k$ could be affected by arbitrarily large variations in the kernel of $\mathbf{K}^{\text{ii}} - \omega_k^2 \mathbf{M}^{\text{ii}}$. However, for a simple eigenvalue, this kernel is one-dimensional and such variations are forbidden by the normalization condition. In this case, the internal modes are necessarily continuous and differentiable.

A multiple eigenvalue can occur if two different eigenvalues cross each other. The differentiability of multiple eigenvalues and of their eigenmodes has been extensively discussed in the structural optimization community, see for instance Haftka *et al.* [37]. Let us consider a system with a one-dimensional configuration space and two eigenvalues, as illustrated in Figure 2. Away from θ^b , the eigenvalues ω_1 and ω_2 and their respective eigenvectors ψ_1 and ψ_2 are well-separated and continuous. At θ^b , we have a double eigenvalue, whose eigenvector is undefined in the subspace spanned by ψ_1 and ψ_2 . Thus, the major pitfall is a permutation phenomenon, which will actually occur if the eigenvectors are sorted and selected according to their eigenvalues:

$$\begin{aligned} \Psi^{\text{iu}}(\theta_1) &= [\psi_1 \quad \psi_2], & \forall \theta_1 < \theta^b \\ \Psi^{\text{iu}}(\theta_1) &= [\psi_2 \quad \psi_1], & \forall \theta_1 > \theta^b \end{aligned}$$

This discussion can be extended for a s -dimensional configuration space, and we conclude that a refinement in the computation of the internal modes is necessary to avoid permutations.

Our algorithm is initialized at a germ configuration where the eigenmodes are sorted and selected according to their eigenvalues. From this germ, it gradually progresses in the whole configuration space Ω_θ , but the eigenmodes are then sorted and selected according to a *mode tracking strategy*, as suggested by Kim and Kim [38]. These authors have exploited the Modal Assurance Criterion (MAC value) which is a measure from 0 to 1 of the correlation between two modes, a unitary value meaning perfect correlation. The correlation is realized between the eigenmodes at the current configuration and at a reference configuration. More precisely, the MAC matrix, which is filled with the MAC numbers of all pairs of modes, is rendered as close as possible to the identity.

The internal modes can only be validated if the deviation of the MAC-matrix from the identity satisfies a tolerance condition. For example, if the reference configuration is far from the current configuration, the correlation may be poor and the consistency cannot be guaranteed. In this case, the procedure should be restarted with a closer reference configuration, as will be explained in section 5.2.

3.4.5 Conclusion

From this consistency analysis, we conclude that *the Global Modal Parameterization (13) is well-defined, provided that a mode-tracking strategy is implemented.* Hence, the GMP defines

a reduction procedure in the sense of section 2.3. The reduced equations of motion and the reduction algorithm are developed in the next section.

4 REDUCED-ORDER MODEL

From the definition of the GMP, the reduced equations of motion (6) can be derived, but the general transformation relations (7) to (11) hide very complex expressions. However, in flexible multibody dynamics, the small deformation assumption allows to omit higher-order contributions of $\boldsymbol{\delta}$, which considerably simplifies the formulation of the elastic and inertia forces.

4.1 Elastic forces

The elastic potential energy is a strongly nonlinear function $\mathcal{V}(\mathbf{q})$, and we seek for an approximation in terms of the reduced coordinates $\boldsymbol{\theta}$ and $\boldsymbol{\delta}$. For small deformations, we have the following result, demonstrated in [36]:

$$\mathcal{V}_{,\eta} = \begin{bmatrix} \mathcal{V}_{,\boldsymbol{\theta}} \\ \mathcal{V}_{,\boldsymbol{\delta}} \end{bmatrix} \simeq \begin{bmatrix} \mathbf{0} \\ \mathbf{K}^{\delta\delta}(\boldsymbol{\theta}) \boldsymbol{\delta} \end{bmatrix} \quad (22)$$

where $\mathbf{K}^{\delta\delta}(\boldsymbol{\theta})$ is defined at the undeformed configuration $\boldsymbol{\rho}(\boldsymbol{\theta})$:

$$\mathbf{K}^{\delta\delta} = (\boldsymbol{\Psi}^{\mathbf{q}\delta})^T \mathbf{K}_t^{\mathbf{q}\mathbf{q}} \boldsymbol{\Psi}^{\mathbf{q}\delta} = \begin{bmatrix} \mathbf{K}^{\gamma\gamma} & \mathbf{0} \\ \mathbf{0} & \boldsymbol{\Omega}^2 \end{bmatrix}$$

$\mathbf{K}^{\gamma\gamma}$ is the $n^{\mathbf{g}} \times n^{\mathbf{g}}$ symmetric stiffness matrix associated with the constraint modes, and $\boldsymbol{\Omega}^2 = \text{diag}\{\omega_i^2\}$ is the diagonal matrix of the n^t squared internal eigenvalues.

4.2 Inertia forces

Theoretically, the reduced mass matrix and Christoffel symbol depend on the whole set of modal parameters $\boldsymbol{\eta}$. However, the dependence with respect to the flexible coordinates $\boldsymbol{\delta}$ can be neglected, so that the inertia forces become:

$$\frac{d}{dt} \left(\frac{\partial \mathcal{K}}{\partial \dot{\boldsymbol{\eta}}} \right) - \frac{\partial \mathcal{K}}{\partial \boldsymbol{\eta}} \simeq \mathbf{M}^{\eta\eta}(\boldsymbol{\theta}) \ddot{\boldsymbol{\eta}} + \mathbf{h}^{\eta}(\boldsymbol{\theta}, \dot{\boldsymbol{\eta}}) \quad (23)$$

with

$$(h^{\eta})_i = (\Gamma^{\eta\eta\eta}(\boldsymbol{\theta}))_{ijk} \dot{\eta}_j \dot{\eta}_k$$

Again, the computation of $\mathbf{M}^{\eta\eta}$ and $(\Gamma^{\eta\eta\eta})_{ijk}$ is only needed at an undeformed configuration. Equations (9), (11) and (15) lead to:

$$\begin{aligned} \mathbf{M}^{\eta\eta} &= (\boldsymbol{\Psi}^{\mathbf{q}\eta})^T \mathbf{M}^{\mathbf{q}\mathbf{q}} \boldsymbol{\Psi}^{\mathbf{q}\eta} \\ (\Gamma^{\eta\eta\eta})_{ijk} &= \underbrace{(\boldsymbol{\Psi}^{\mathbf{q}\eta})_{ui} (\boldsymbol{\Psi}^{\mathbf{q}\eta})_{vj} (\boldsymbol{\Psi}^{\mathbf{q}\eta})_{wk} (\Gamma^{qqq})_{uvw}}_{\equiv (\widetilde{\Gamma^{\eta\eta\eta}})_{ijk}} + \underbrace{(\boldsymbol{\Psi}^{\mathbf{q}\eta})_{ui} \frac{\partial^2 q_v}{\partial \eta_j \partial \eta_k} (M^{qq})_{uv}}_{\equiv (\overline{\Gamma^{\eta\eta\eta}})_{ijk}} \end{aligned}$$

Using (16), $\widetilde{\Gamma^{\eta\eta\eta}}$ can be computed from a sensitivity analysis of the mode shapes with respect to $\boldsymbol{\theta}$, according to a finite difference approach. In our finite element formulation, the Christoffel symbol $(\Gamma^{qqq})_{uvw}$ is not directly available, and its expression cannot be used explicitly for the computation of $(\widetilde{\Gamma^{\eta\eta\eta}})_{ijk}$. For this reason, we propose an algorithm for $(\overline{\Gamma^{\eta\eta\eta}})_{ijk}$ which only involves the computation of the forces $\mathbf{h}^{\mathbf{q}}$. Let us define $\overline{\mathbf{h}}^{\eta}$

$$(\overline{\mathbf{h}}^{\eta})_i = (\overline{\Gamma^{\eta\eta\eta}})_{ijk} \dot{\eta}_j \dot{\eta}_k$$

At an undeformed configuration, it is easily verified that: $\overline{\mathbf{h}}^{\eta} = (\boldsymbol{\Psi}^{\mathbf{q}\eta})^T \mathbf{h}^{\mathbf{q}}$. For a given $\dot{\boldsymbol{\eta}}$, $\overline{\mathbf{h}}^{\eta}$ can thus be computed in the following way:

1. Compute $\dot{\mathbf{q}} = \Psi^{\mathbf{q}\eta} \dot{\boldsymbol{\eta}}$
2. Compute $\mathbf{h}^{\mathbf{q}}$ (initial model)
3. Deduce $\overline{\mathbf{h}}^{\eta} = (\Psi^{\mathbf{q}\eta})^T \mathbf{h}^{\mathbf{q}}$

From this observation, all coefficients $(\overline{\Gamma^{\eta\eta\eta}})_{ijk}$ can be identified from two series of tests when zero or unit velocities are imposed to appropriate modal coordinates:

- Identification of the “diagonal” terms $(\overline{\Gamma^{\eta\eta\eta}})_{iaa}$ ($a = 1, \dots, n^{\eta}$). Impose $\dot{\eta}_a = 1$, and use:

$$(\overline{h}^{\eta})_i = (\overline{\Gamma^{\eta\eta\eta}})_{iaa} \quad (\text{no sum for } a)$$

- Identification of the “off-diagonal” terms $(\overline{\Gamma^{\eta\eta\eta}})_{iab}$ ($a = 1, \dots, n^{\eta}$ and $b = a + 1, \dots, n^{\eta}$). Impose $\dot{\eta}_a = \dot{\eta}_b = 1$, and use:

$$(\overline{h}^{\eta})_i = (\overline{\Gamma^{\eta\eta\eta}})_{iaa} + (\overline{\Gamma^{\eta\eta\eta}})_{ibb} + 2 (\overline{\Gamma^{\eta\eta\eta}})_{iab} \quad (\text{no sum for } a \text{ nor for } b)$$

4.3 Reduced equations of motion

Considering that the external loads are transformed according to (8) and (15):

$$\mathbf{g}^{\eta} = \Psi^{\mathbf{q}\eta T} \mathbf{g}^{\mathbf{q}}$$

the reduced equations of motion follow:

$$\boxed{\mathbf{M}^{\eta\eta}(\boldsymbol{\theta}) \ddot{\boldsymbol{\eta}} + \mathbf{h}^{\eta}(\boldsymbol{\theta}, \dot{\boldsymbol{\eta}}) + \mathbf{K}^{\eta\eta}(\boldsymbol{\theta}) \boldsymbol{\eta} = \mathbf{g}^{\eta}} \quad (24)$$

with the structure:

$$\mathbf{M}^{\eta\eta} = \begin{bmatrix} \mathbf{M}^{\theta\theta} & \mathbf{M}^{\theta\gamma} & \mathbf{M}^{\theta\iota} \\ \mathbf{M}^{\gamma\theta} & \mathbf{M}^{\gamma\gamma} & \mathbf{M}^{\gamma\iota} \\ \mathbf{M}^{\iota\theta} & \mathbf{M}^{\iota\gamma} & \mathbf{I} \end{bmatrix}, \quad \mathbf{K}^{\eta\eta} = \begin{bmatrix} \mathbf{0} & \mathbf{0} & \mathbf{0} \\ \mathbf{0} & \mathbf{K}^{\gamma\gamma} & \mathbf{0} \\ \mathbf{0} & \mathbf{0} & \Omega^2 \end{bmatrix}, \quad \mathbf{g}^{\eta} = \begin{bmatrix} \mathbf{g}^{\mathbf{a}} + (\Psi^{\mathbf{g}\theta})^T \mathbf{g}^{\mathbf{g}} \\ \mathbf{g}^{\mathbf{g}} \\ \mathbf{0} \end{bmatrix}$$

$\mathbf{g}^{\mathbf{a}}$ denotes the actuator forces and $\mathbf{g}^{\mathbf{g}}$ the forces applied to the constraint dofs. This model is fully described by $\mathbf{M}^{\eta\eta}$, $\mathbf{K}^{\eta\eta}$, $(\Gamma^{\eta\eta\eta})_{ijk}$ and $\Psi^{\mathbf{g}\theta}$, which smoothly depend on $\boldsymbol{\theta}$. The model (24) has the Lagrangian structure provided that the approximations (22) and (23) are acceptable, i.e. that the deformations are sufficiently small.

4.4 Algorithm for local model reduction

Assuming that a reference model is available at a configuration $\boldsymbol{\theta}_{ref}$ (with local modes Ψ_{ref}), the numerical construction of the reduced-order model (24) for a configuration $\boldsymbol{\theta} \in \Omega_{\boldsymbol{\theta}}$ is described in Figure 3. This local analysis is combined with a configuration space approximation algorithm, presented in the next section. Hence, a database is exploited to store and reuse the local models. As mentioned earlier, the mode matching may fail if the reference configuration $\boldsymbol{\theta}_{ref}$ is too far from $\boldsymbol{\theta}$, leading to a non-valid model.

5 APPROXIMATION IN THE CONFIGURATION SPACE

The local construction of the reduced-order model involves a computationally demanding numerical procedure. However, the variations of the model in the configuration space can be explicitly described by a simplified and approximated metamodel, or model of the model. If all relevant coefficients associated with $\mathbf{M}^{\eta\eta}$, $\mathbf{K}^{\eta\eta}$, $(\Gamma^{\eta\eta\eta})_{ijk}$ and $\Psi^{\mathbf{g}\theta}$ are collected in a single

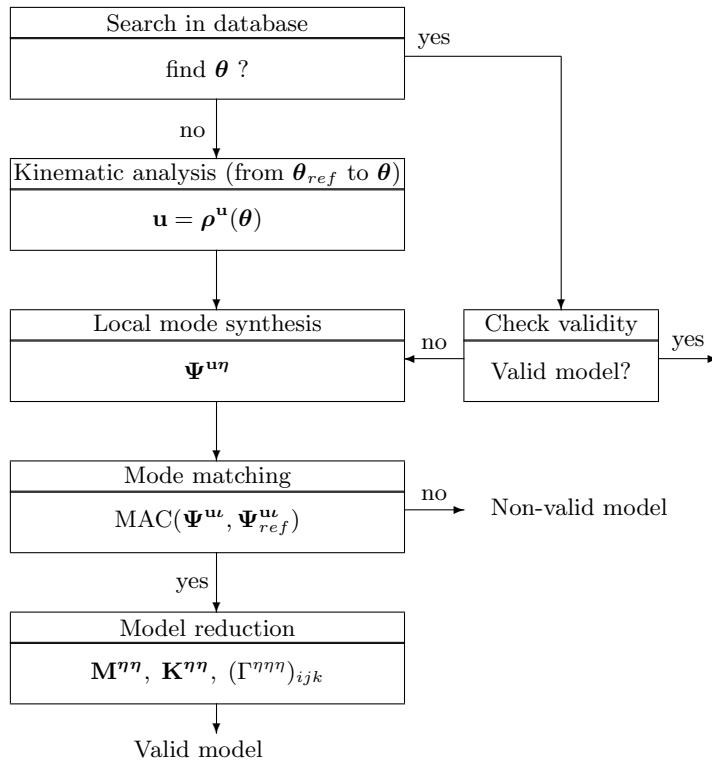


Figure 3: Construction of the reduced model locally at configuration θ .

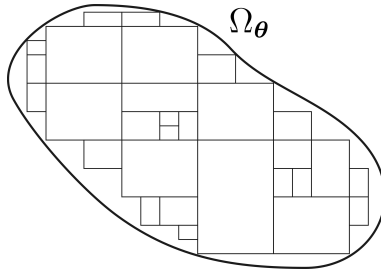


Figure 4: Decomposition of a two-dimensional configuration space Ω_{θ} into a collection of boxes.

$t \times 1$ output vector \mathbf{f} , the numerical reduction procedure is a smooth black box function $\mathbf{f}(\boldsymbol{\theta})$, and the metamodel is an approximation $\tilde{\mathbf{f}}(\boldsymbol{\theta})$ for this function:

$$\tilde{\mathbf{f}}(\boldsymbol{\theta}) \simeq \mathbf{f}(\boldsymbol{\theta}), \quad \forall \boldsymbol{\theta} \in \Omega_{\theta}$$

Clearly, there is a trade-off between the accuracy of the approximation and the complexity of the metamodel. In general, the metamodel is elaborated in two steps: (i) for a selected set of configurations $\boldsymbol{\theta}^{(k)}$ ($k = 1, \dots, n^{cfg}$), the local models $\mathbf{f}^{(k)}$ are computed, (ii) the function $\tilde{\mathbf{f}}(\boldsymbol{\theta})$ is fitted on those data.

In this research, we consider low-order polynomial approximations, which are simple yet efficient for our applications. In order to increase the flexibility of the approximation, a *piecewise strategy* is adopted. As illustrated in figure 4, this means that the configuration space is decomposed into several non-overlapping boxes for which local polynomials are defined. This decomposition can be realized adaptively in order to satisfy a specification on the approximation error. Thus, a general, efficient and systematic approximation procedure is developed leading to a portable and computationally efficient nonlinear model.

The next sections briefly discuss the local polynomial approximation and the automatic configuration space decomposition. Additional information can be found in [36].

5.1 Local polynomial approximation

Let us consider the quadratic polynomial defined by:

$$P_s = a + \sum_{i=1}^s b_i \theta_i + \sum_{i=1}^s \sum_{j=i}^s c_{ij} \theta_i \theta_j$$

In a s -dimensional box, the data points $\boldsymbol{\theta}^{(k)}$ can be selected according to the central composite design (Figure 5a), since it provides sufficient information to fit all coefficients a , b_i and c_{ij} .

Using piecewise quadratic polynomials, the approximation function exhibits a discontinuous behaviour at every boundary between boxes. This drawback can be overcome using the family of Lagrange polynomials [40, 41], which have two interesting properties: (i) the interpolation is exact at the data points, (ii) continuity is obtained at every boundary between boxes with matching grid points. However, if an adaptive strategy is implemented for the configuration space decomposition, this second property is lost, as illustrated in Figure 5b.

For dimensions $s = 1$ to 6, Table 1 compares quadratic and Lagrange approximations for a function $f : \mathcal{R}^s \rightarrow \mathcal{R}$ with respect to the number of operations n^{op} to compute the value of \tilde{f} for a given $\boldsymbol{\theta}$, the size of the data-base n^{db} required to store the metamodel, and the number of data points n^{cfg} necessary to fit the approximation. We observe that Lagrange polynomials are less attractive for high-dimensional problems.

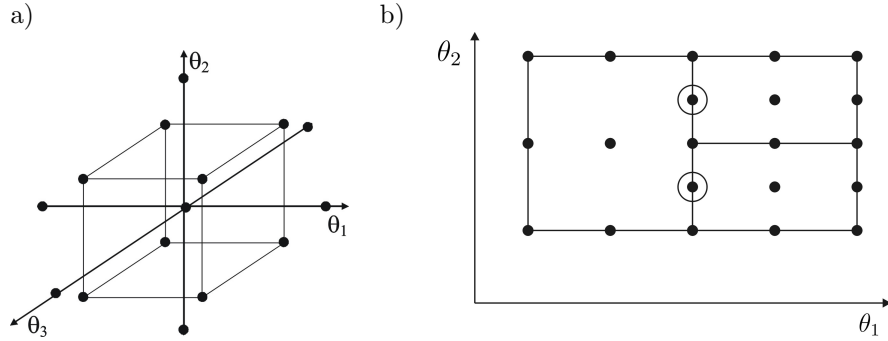


Figure 5: a) Central composite designs in 3D space [39]. b) Discontinuity of Lagrange polynomials between boxes with non-matching grids: the circled points do not belong to the grid of the left box.

Table 1: Comparison between quadratic and Lagrange polynomials.

s	n^{op}		n^{db}		n^{cfg}	
	Quadratic	Lagrange	Quadratic	Lagrange	Quadratic	Lagrange
1	4	4	3	3	5	3
2	10	16	6	9	9	9
3	18	52	10	27	15	27
4	28	160	15	81	25	81
5	40	484	21	243	43	243
6	54	1456	28	729	77	729
s	$s^2 + 3s$	$2(3^s - 1)$	$\frac{s^2+3s+2}{2}$	3^s	$2^s + 2s + 1$	3^s

5.2 Automatic configuration space decomposition

For a better compromise between accuracy, continuity, memory storage and efficient construction of the approximation function, the size of the boxes should be adapted according to the local behaviour of \mathbf{f} . For instance, close to singularities, a refinement is suitable to track the strong variations of the dynamic parameters.

Algorithm 1 buildModel(box, tolError)

```

find the reference configuration  $\theta_{ref}$ 
for  $k = 1$  to  $n^{cfg}$  do
    build the local model  $\mathbf{f}^{(k)}$  at configuration  $\theta^{(k)}$  (Figure 3)
end for
if valid local models then
    build the approximation  $\widehat{\mathbf{f}}(\theta)$ 
    analysis of the approximation error: error
    if error < tolError then
        return
    end if
end if
[leftChildBox, rightChildBox] = box.bisect()
buildModel(leftChildBox, tolError)
buildModel(rightChildBox, tolError)

```

The construction of the global model follows the recursive Algorithm 1, which relies on the representation of the configuration space as a binary tree data structure. For a given root box included in Ω_θ , the tree is automatically constructed by successive bisections and recursive calls. The bisection stops when an estimate of the relative approximation error satisfies a user-defined tolerance. At the end of the algorithm, the model is thus available for any point in the root box with an acceptable precision. More details about the error analysis and the selection of the bisection direction are described in [36]. This algorithm can be easily adapted if the configuration space is not initially represented by a unique root box but by a collection of root boxes.

The reference configuration needed for the local reduction procedure can be any previously computed and validated configuration. Provided that an proper germ configuration is initially defined, our implementation of Algorithm 1 guarantees that a reference configuration can always be found in the current box. Therefore, the problem of remote reference configurations is automatically solved by bisection into smaller boxes.

Remark: Curse of dimensionality.

One may object that the size of the database and the computational effort to build the reduced-order model increase exponentially with respect to the dimension of the configuration space. However, in many control applications, the desired trajectory of the mechanism is known in advance. The inspection strategy can then be restricted to the configurations along the trajectory, which are parameterized using the arclength or a pseudo-time variable. The approximation then becomes a one-dimensional problem, that can be solved with a high efficiency.

Remark: Additional parameters of the model.

In addition to the components of $\mathbf{M}^{\eta\eta}$, $(\Gamma^{\eta\eta\eta})_{ijk}$, $\mathbf{K}^{\eta\eta}$ and $\Psi^{\mathbf{g}\theta}$, the vector \mathbf{f} can include any other relevant information, such as the modal contributions of the gravity forces or the amplitudes of the mode shapes at a sensor coordinate.

Remark: Implementation.

The reduction algorithm has been implemented in the Oofelie industrial software [42]. The module dedicated to flexible multibody dynamics is based on the finite element method described by G eradin and Cardona [1].

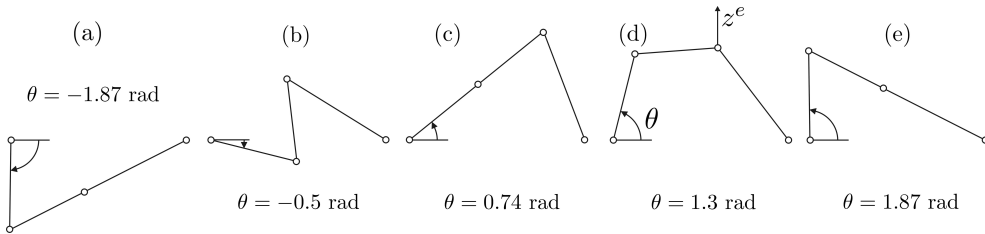


Figure 6: Large configuration changes of the four-bar mechanism.

6 EXAMPLES

6.1 Four-bar mechanism

Figure 6 represents a four-bar mechanism with large configuration changes. The mechanism is controlled by a motor at the lower left hinge, so that the rigid motion is parameterized using the hinge angle θ . Configurations (a) and (e) are actuator singularities, and they define the limits of our study in the configuration space (actually, the configuration space of interest is restricted to $\theta \in [-1.75, 1.75]$ rad). At the singular configurations, the actuator is not able to control the motion of the mechanism, and the aligned links may bend upward or downward, depending on other external forces.

We consider that the operations of a tool cause vertical loads on the upper right hinge, and one constraint mode is therefore associated with the vertical displacement z^e of that point. Three internal modes are also selected to represent the deformations of the mechanism. The initial finite element model contains 84 generalized coordinates and 7 Lagrange multipliers, whereas the reduced model involves 5 modal coordinates (1 rigid mode, 1 constraint mode, 3 internal modes), which are represented for configuration (d) in Figure 7. Two internal modes have an out-of-plane deformation. For this one-dimensional configuration space, the Lagrange interpolation technique is selected and different versions of the reduction algorithm are tested.

First, the configuration space is decomposed into 32 regular boxes, and the mode tracking algorithm is disabled. The natural frequencies of the selected internal modes are plotted in Figure 8, on the left. The algorithm selects the three modes with the lowest frequencies, so that non-smooth variations are observed whenever an eigenvalue crossing occurs. The perturbations around $\theta = 0.7$ rad are attributed to the fourth internal mode, whose natural frequency drops at configuration (c). This situation is of course not acceptable, since it leads to a non-consistent parameterization of the motion. The mode tracking strategy is able to remedy this situation, as attested by the results on the right plot in Figure 8.

For the components associated with the rigid mode, Figure 9 illustrates the variations of the mass matrix and Christoffel symbol in the configuration space. A vertical asymptote is expected close to the extreme singular configurations. Mathematically, the components of the rigid modes grow to infinity at those points, which explains the phenomenon. From the actuator point of view, the mechanical blocking at the singularity is equivalent to an infinite inertia. It is also observed that the Christoffel symbol is connected with the gradient of the mass matrix, in agreement with equation (2).

Then, the adaptive decomposition is considered, leading to a set of 37 irregular boxes (only 5 more than for the regular grid). Figure 10 compares the relative approximation errors:

$$err_i(\theta) = \frac{\|f_i(\theta) - \hat{f}_i(\theta)\|}{\|f_i(\theta)\|}$$

At the singularity, low-order polynomials defined on a regular grid are not able to represent efficiently the strongly nonlinear behaviour of the system. Due to a refinement of the grid close

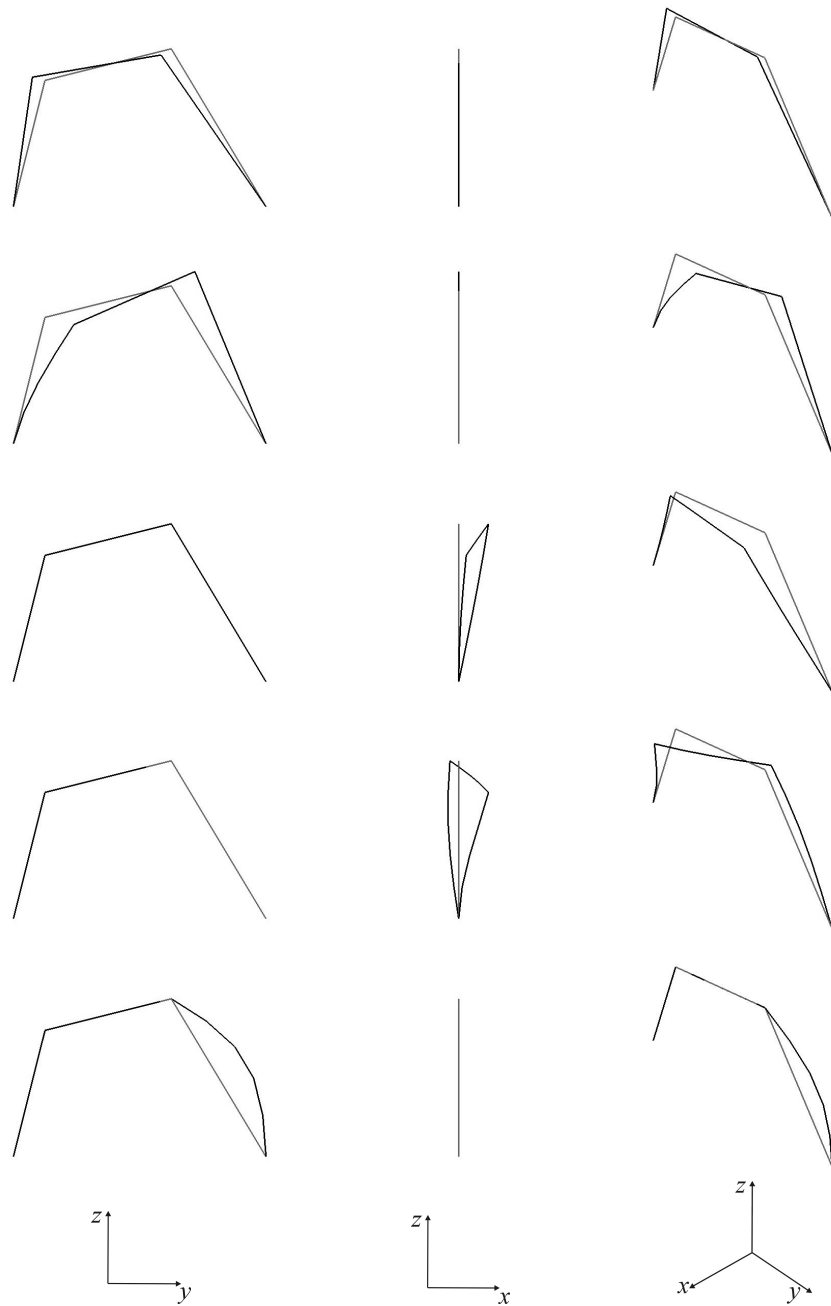


Figure 7: Mode shapes for configuration (d). From top to bottom: rigid mode, constraint mode (θ is fixed), and 3 internal modes (θ and z^e are fixed).

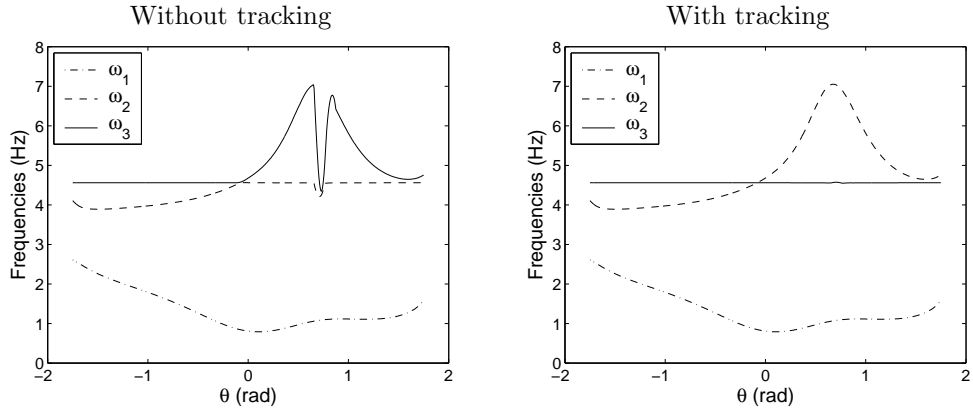


Figure 8: Natural frequencies in the configuration space: importance of the tracking strategy.

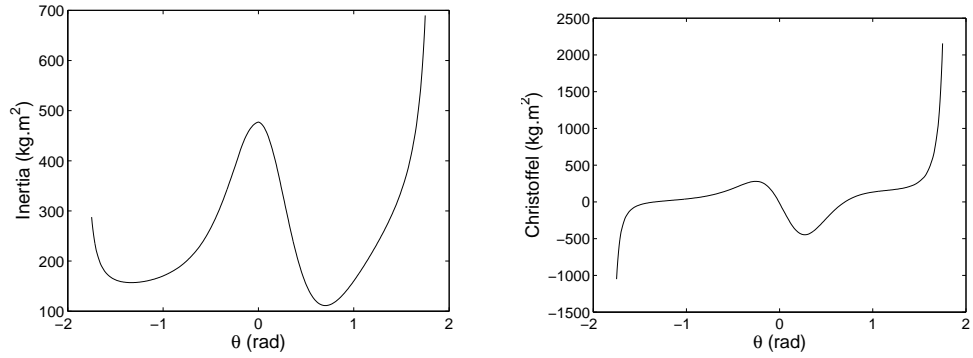


Figure 9: Variations of the equivalent inertia associated with the rigid mode $(M^{\theta\theta})_{11}$, and of the component of the Christoffel symbol $(\Gamma^{\eta\eta\eta})_{111}$.

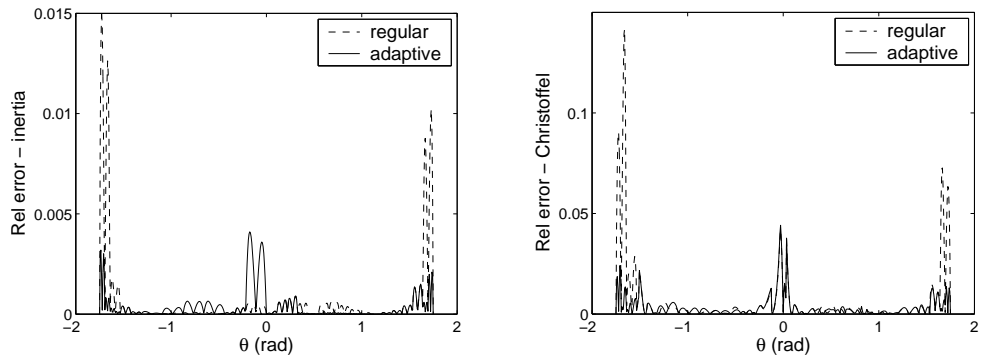


Figure 10: Comparison of the relative errors for regular and adaptive grids.

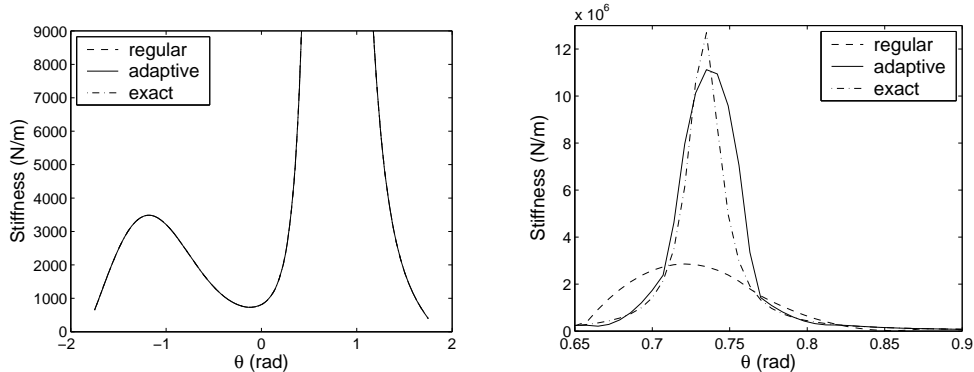


Figure 11: Equivalent stiffness associated with the constraint mode for two different axis ranges.

to the singularity, the adaptive method is able to overcome this difficulty. In other parts of the configuration space, small errors are tolerated allowing a coarser discretization.

The equivalent stiffness associated with the constraint mode is analysed in Figure 11. Close to the singularities, this stiffness decreases to zero, but it takes very large values around configuration (c). At this configuration, the two left links are aligned, and any vertical motion z^e induces traction or compression efforts, involving tremendous strain energy. As a result, the vertical deflection of the effector is almost blocked. The regular grid leads to a rough approximation in a large domain around the peak, which may strongly affect the quality of the model. The adaptive grid is far more efficient.

From this example, we conclude that the variations of the stiffness and inertia parameters in the configuration space receive a consistent physical interpretation, but that the mode-tracking strategy is essential for the reliability of the results. A polynomial approximation can accurately capture the nonlinear changes in the parameters of the model, and the adaptive configuration space decomposition is valuable to reduce the approximation error and to optimize the computational resources.

6.2 Long-reach manipulator

The long-reach manipulator Ralf, shown in Figure 12, has been developed at the IMDL research center of the Georgia Institute of Technology [43, 44]. It operates in a vertical plane and the two kinematic dofs are controlled by hydraulic actuators. The structure consists of two main links (3.05 m long) and a parallel actuation mechanism. Ralf has a high payload to weight ratio, and it is stiff enough to achieve real-world applications. However, flexible phenomena affect the positioning accuracy.

The first actuator moves the first link relative to the base, the second moves the second link relative to the first through the parallel mechanism. Two linear position sensing transducers, fixed to the hydraulic cylinder, measure the cylinder extension. Moreover, in order to detect the vibrations of the mechanism, two accelerometers have been placed at the tip, in two orthogonal directions. As seen in Figure 12, the rigid configuration of Ralf can be described either using the relative angles α_1 and α_2 of the main links, or the actuator extensions θ_1 and θ_2 .

The two main links and the actuator link are modelled using flexible beam elements, all other components are considered as rigid-bodies, lumped masses and ideal joints. The initial finite element model involves 140 generalized coordinates and 24 Lagrange multipliers.

For the reduction, 2 rigid modes and 2 flexible modes (Figure 13) turned out to be sufficient to capture the essential dynamic behaviour of the system in the frequency range 0-15 Hz. Higher-order modes are above 30 Hz, and their participation to the dynamic response is neglected.

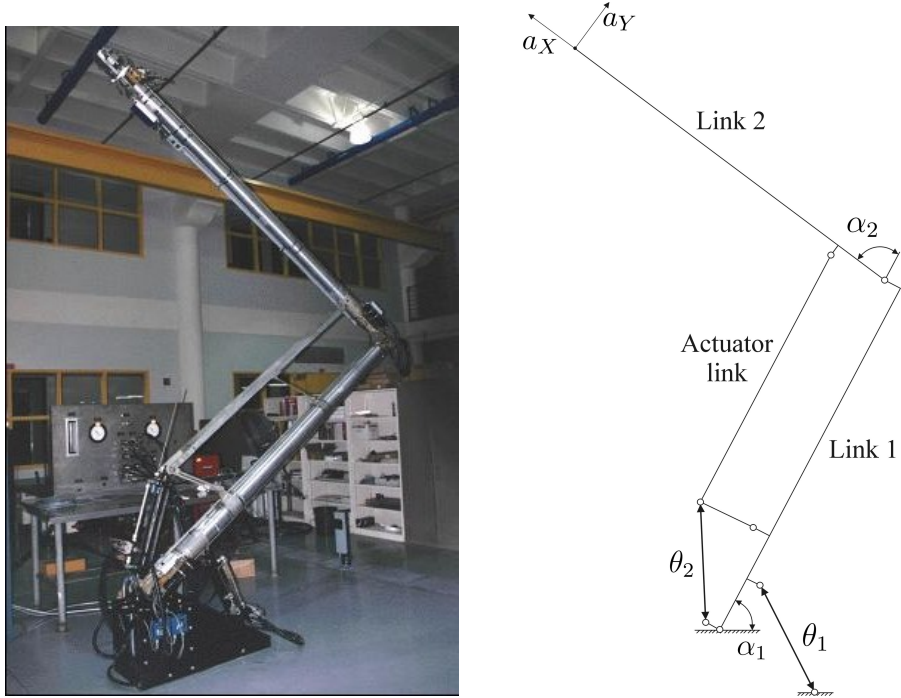


Figure 12: Ralf, coordinates of the actuators and sensors.

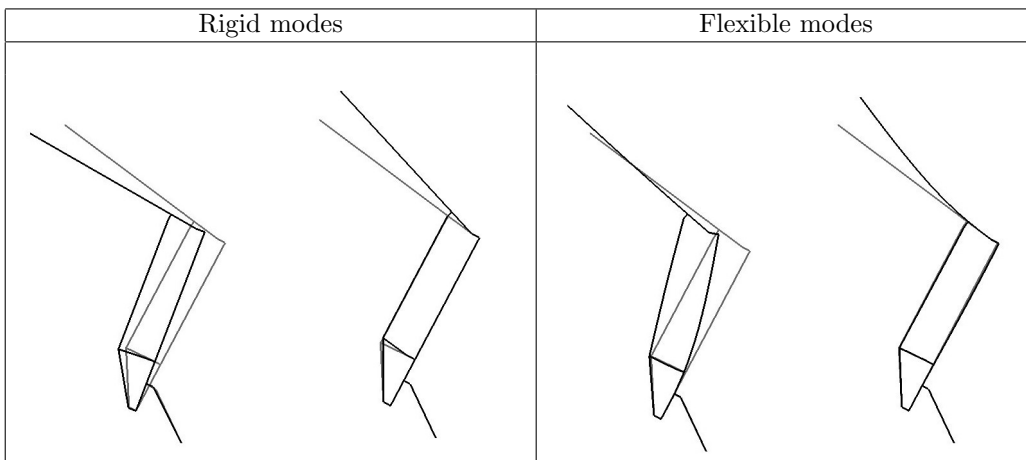


Figure 13: Mode shapes, home configuration.

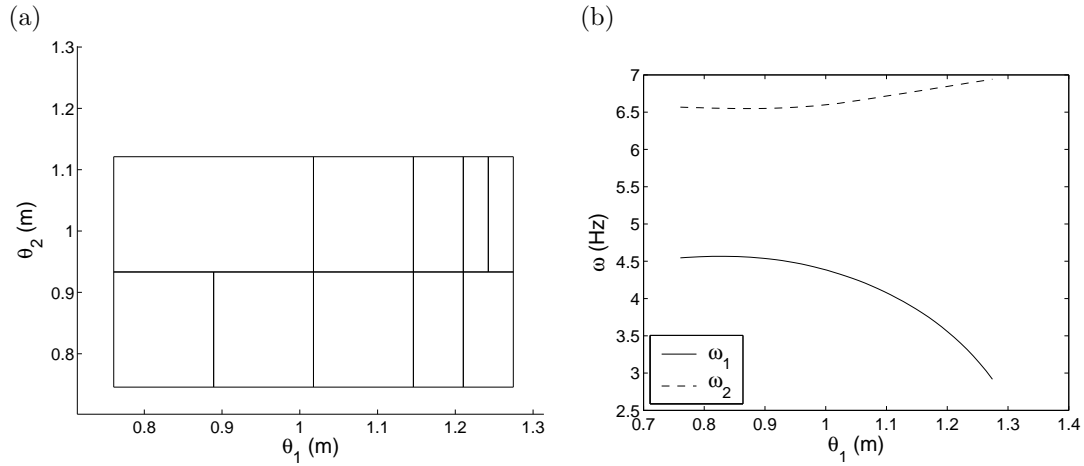


Figure 14: (a) Configuration space discretization. (b) Variations of the natural frequencies along a diagonal line in the configuration space from the lower left corner to the upper right corner.

According to Lee [45], the gyroscopic forces are negligible for this manipulator. Therefore, the reduced equations of motion are in linear parameter varying form:

$$\begin{bmatrix} \mathbf{M}^{\theta\theta}(\theta) & \mathbf{M}^{\theta\delta}(\theta) \\ \mathbf{M}^{\delta\theta}(\theta) & \mathbf{I} \end{bmatrix} \begin{bmatrix} \ddot{\boldsymbol{\theta}} \\ \ddot{\boldsymbol{\delta}} \end{bmatrix} + \begin{bmatrix} \mathbf{0} & \mathbf{0} \\ \mathbf{0} & \boldsymbol{\Omega}^2(\theta) \end{bmatrix} \begin{bmatrix} \boldsymbol{\theta} \\ \boldsymbol{\delta} \end{bmatrix} = \begin{bmatrix} \mathbf{g}^a \\ \mathbf{0} \end{bmatrix}$$

A piecewise Lagrange approximation is selected; the configuration space discretization and the variations of the natural frequencies are illustrated in Figure 14.

The relation between the end effector position \mathbf{x}^e and the modal coordinates is:

$$\mathbf{x}^e = \boldsymbol{\rho}^e(\theta) + \boldsymbol{\Psi}^{e\delta}(\theta) \boldsymbol{\delta}$$

where $\boldsymbol{\rho}^e$ is the kinematic transformation of the rigid mechanism (which is available in analytical form), and $\boldsymbol{\Psi}^{e\delta}$ is the 2×2 matrix of the flexible modes at the effector.

Around a fixed configuration, a frequency-domain analysis is possible for the linearized system. For experimental validation, a model of the hydraulic actuators has also been developed and some parameters have been identified. The structural damping has been adjusted to a value around 1 % (actually, the dominant damping effect in the overall system comes from the actuators and the control system). A comparison between the resulting model and experimental results is given in Figure 15. Some discrepancies can be observed, which are attributed to the weaknesses of the identification procedure. Nevertheless, we conclude that a reduced-order model is able to capture the configuration-dependent dynamics of a real manipulator.

This model has been exploited for the development of a position and vibration controller based on a two-time-scale strategy: the slow controller is a classical joint-tracking controller, while the fast controller realizes the active damping of the vibrations. The vibration control law relies on a real time implementation of the reduced-order model, and its efficiency clearly appears in Figure 16. A full discussion about the modelling and control of Ralf can be found in [36].

7 SUMMARY AND CONCLUSIONS

A nonlinear model reduction technique has been presented for the compact and closed-form representation of flexible multibody systems with parallel topology. The method relies on the following assumptions:

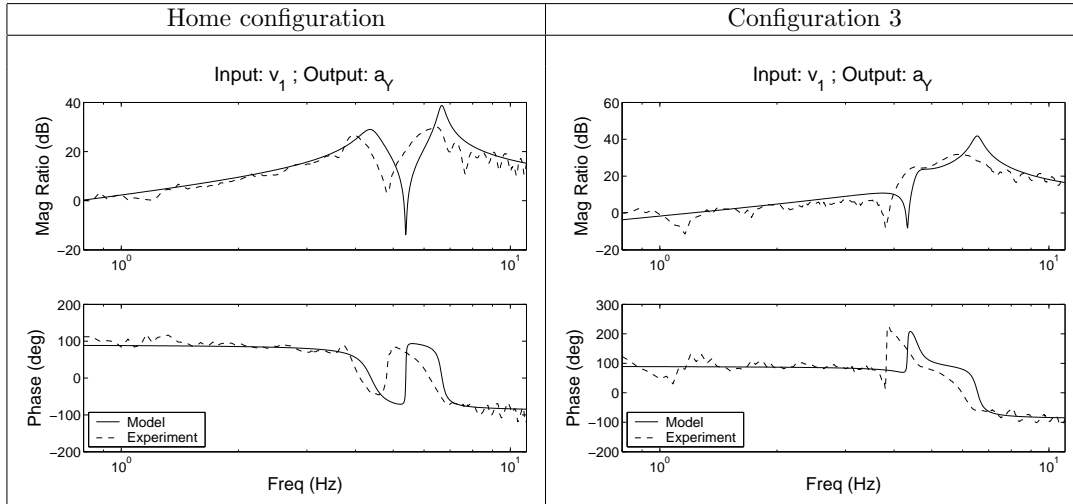


Figure 15: Experimental and model transfer functions (from actuator voltage to tip acceleration), for two different configurations.

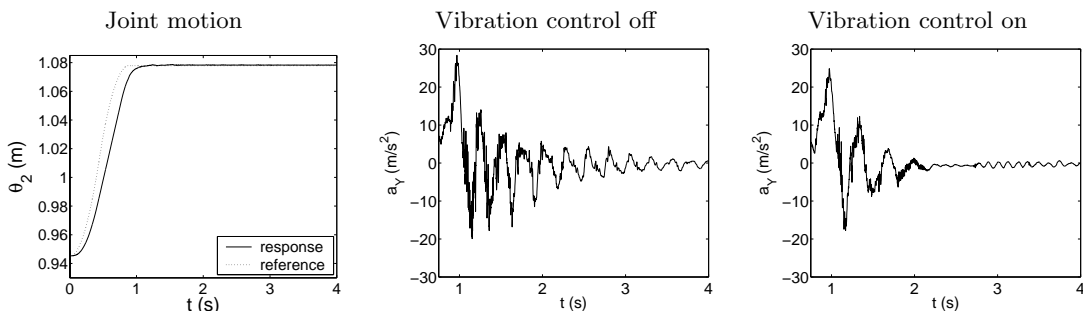


Figure 16: Experimental results for a point-to-point trajectory: joint motion and tip acceleration. The acceleration plots focus on the final time interval, after reaching the end point.

- the system is conservative and holonomic, no pre-stressing effect is considered,
- the singularities are avoided in the configuration space,
- the deformations are small, the elastic behaviour is linear, and centrifugal stiffening effects are not taken into account.

The reduction is achieved at the mechanism level by projection of the dynamics onto a submanifold of the configuration space. This procedure is formally defined in two steps: (i) a full coordinate transformation into independent modal coordinates, (ii) a truncation of the higher-order flexible modes. In the resulting Global Modal Parameterization, the new coordinates have a clear physical interpretation in terms of rigid and flexible modes, and the actuator coordinates appear explicitly. The reduced-order model still has the Lagrangian structure; the mass matrix, the stiffness matrix, and the Christoffel symbol are configuration-dependent. Their coefficients are represented approximately using piecewise polynomial functions, with the advantages of computational efficiency and portability. In the reduction procedure, the accuracy loss is localized at two levels:

- the truncation of the flexible modal basis (the rigid motion is exactly represented),
- the approximation in the configuration space.

The procedure is systematic and the user only needs to provide high-level information: an initial model of the mechanism (e.g. a finite element model), the partitioning into rigid, constraint, and internal dofs, the number of internal modes, a region of the configuration space, and the tolerance on the approximation error. The mode shapes are selected automatically according to a parametric component-mode synthesis. The technique of Hurty [16] has been selected but this choice is not restrictive: other component-modes proposed in the literature could be later considered. As a special case, the method is applicable to rigid mechanisms; it is then equivalent to the constraint elimination technique described in [46].

Two examples have been successfully analysed: a flexible four-bar mechanism and a flexible manipulator. For the manipulator, an experimental validation has been realized, and the model has been exploited for the design and implementation of a position and vibration controller.

The method could also be used for the offline numerical optimization of a control law (trajectory generation, inverse dynamics, training of a feedback action) or to fit a more structured model (e.g. polytopic linear model [28], model based on linear fractional transformation [29]). In future work, the reduction method will be exploited in order to facilitate a system-level simulation. It would also be interesting to examine the convergence of simulation results with respect to the number of modes in the reduced-model.

Acknowledgements

This work has been supported by the Belgian National Fund for Scientific Research (FNRS) which is gratefully acknowledged. It also presents research results of the Belgian Program on Inter-University Attraction Poles initiated by the Belgian Federal Science Policy Office (AMS IAP V/06). The scientific responsibility rests with its authors. The experimental work on Ralf has been realized in collaboration with Prof. W.J. Book and R. Krauss from the Georgia Institute of Technology in Atlanta; they are gratefully acknowledged.

References

- [1] M. Géradin and A. Cardona. *Flexible Multibody Dynamics: A Finite Element Approach*. John Wiley & Sons: New York, 2001.
- [2] A.A. Shabana. *Dynamics of Multibody Systems* (2nd edn). Cambridge University Press, 1998.

- [3] B.F. De Veubeke. The dynamics of flexible bodies. *Int. J. Engineering Science* 1976; **14**:895–913.
- [4] A.A. Shabana and R.A. Wehage. A coordinate reduction technique for dynamic analysis of spatial substructures with large angular rotations. *J. Struct. Mech.* 1983; **11**:401–431.
- [5] W.J. Book. Recursive Lagrangian dynamics of flexible manipulator arms. *Int. J. Robotics Res.* 1984; **3**(3):87–101.
- [6] A. Cardona and M. Géradin. A superelement formulation for mechanism analysis. *Int. J. Num. Meth. Eng.* 1991; **32**(8):1565–1594, .
- [7] C.L. Bottasso, A. Croce, and D. Leonello. Neural-augmented planning and tracking pilots for maneuvering multibody dynamics. In *Proc. of the ECCOMAS Conf. on Advances in Computational Multibody Dynamics*, Madrid, Spain, June 2005.
- [8] B.C. Moore. Principal component analysis in linear systems: Controllability, observability and model reduction. *IEEE Trans. Autom. Control* 1981; **26**:17–32.
- [9] K.D. Glover. All optimal Hankel-norm approximation of linear multivariable systems and their L^∞ -error bounds. *Int. J. Control* 1984; **39**(6):1115–1193.
- [10] D.C. Sorensen and A.C. Antoulas. The sylvester equation and approximate balanced reduction. *Linear Algebra and its Applications* 2002; **351-352**:671–700.
- [11] E.J. Grimme. *Krylov projection methods for model reduction*. PhD thesis, ECE Department, Univ. Of Illinois, Urbana-Champaign, 1997.
- [12] K. Gallivan, A. Vandendorpe, and P. Van Dooren. Model reduction of MIMO systems via tangential interpolation. *SIAM J. Matrix Analysis and Applications* 2004; **26**(2):328–349.
- [13] T.J. Su and R.J. Craig. Model reduction and control of flexible structures using Krylov vectors. *AIAA J. Guidance, Control, and Dynamics* 1991; **14**(2):260–267.
- [14] D.G. Meyer and S. Srinivasan. Balancing and model reduction for second-order form linear systems. *IEEE Trans. Autom. Control* 1996; **41**(11):1632–1644.
- [15] Z. Bai and Y. Su. Dimension reduction of large-scale second-order dynamical systems via a second-order Arnoldi method. *SIAM J. Sci. Comput.* 2005; **26**(5):1692–1709.
- [16] W.C. Hurty. Dynamic analysis of structural systems using component modes. *AIAA J.* 1965; **3**(4):678–685.
- [17] R. Craig and M. Bampton. Coupling of substructures for dynamic analysis. *AIAA J.* 1968; **6**(7):1313–1319.
- [18] R. Mac Neal. A hybrid method of component mode synthesis. *Computers and Structures* 1975; **1**:581–601.
- [19] S. Rubin. Improved component mode representation for structural dynamics analysis. *AIAA J.* 1975, **13**(8):995–1006.
- [20] R. Craig. A review of time-domain and frequency domain component-mode synthesis methods. *Int. J. Analytical and Experimental Modal Analysis* 1987; **11**(6):562–570.
- [21] M. Géradin and D. Rixen. *Mechanical Vibrations: Theory and Application to Structural Dynamics* (2nd edn). John Wiley & Sons: New York, 1997.
- [22] K. Pearson. On lines and planes of closest fit to points in space. *Philosophical Magazine* 1901; **2**:609–629.

- [23] S. Lall, J.E. Marsden, and S. Glavaski. A subspace approach to balanced truncation for model reduction of nonlinear control systems. *Int. J. Robust Nonlinear Control* 2002; **12**:519–535.
- [24] M.J. Rewienski. *A Trajectory Piecewise-Linear Approach to Model Order Reduction of Nonlinear Dynamical Systems*. PhD thesis, Massachusetts Institute of Technology, 2003.
- [25] T. Takagi and M. Sugeno. Fuzzy identification of systems and its applications to modeling and control. *IEEE Trans. Syst., Man, Cybern.* 1985; **15**:116–132.
- [26] O. Nelles. *Nonlinear System Identification with Local Linear Neuro-Fuzzy Models*. PhD thesis, TU Darmstadt, 1999.
- [27] R. Murray-Smith. *A Local Model Network Approach to Nonlinear Modelling*. PhD thesis, University of Strathclyde, Department of Computer Science, Glasgow, Scotland, November 1994.
- [28] G.Z. Angelis. *System Analysis, Modelling and Control with Polytopic Linear Models*. PhD thesis, Technische Universiteit Eindhoven, 2001.
- [29] C.W. Scherer. LPV control and full block multipliers. *Automatica* 2001; **37**:361–375.
- [30] J. Scherpen. Balancing for nonlinear systems. *System & Control Letters* 1993; **21**:143–153.
- [31] M.H. Raibert. Analytical equations vs. table look-up for manipulation: a unifying concept. In *Proc. of the IEEE Conf. Decision and Control*, New Orleans, 1977.
- [32] J.G. Papastavridis. *Tensor Calculus and Analytical Dynamics*. CRC Press: Florida, 1998.
- [33] F.C. Park and J.W. Kim. Singularity analysis of closed kinematic chains. *ASME J. Mech. Des.* 1999; **121**(1):32–38.
- [34] D. Zlatanov, I. Bonev, and C. Gosselin. Constraint singularities as configuration space singularities, 2001. <http://www.parallemic.org/Reviews/Review008.html> [5 May 2006].
- [35] G. Liu, Y. Lou, and Z. Li. Singularities of parallel manipulators: A geometric treatment. *IEEE Trans. Robotics and Automation* 2003; **19**(4):579–594.
- [36] O. Brüls. *Integrated Simulation and Reduced-Order Modeling of Controlled Flexible Multi-body Systems*. PhD thesis, University of Liège, Belgium, 2005.
- [37] R.T. Haftka, Z. Gürdal, and M.P. Kamat. *Elements of Structural Optimization* (2nd edn). Kluwer Academic Publishers: Dordrecht, The Netherlands, 1990.
- [38] T.S. Kim and Y.Y. Kim. MAC-based mode-tracking in structural topology optimization. *Computers and Structures* 2000; **74**:375–383.
- [39] D.C. Montgomery. *Design and Analysis of Experiments* (4th edn). John Wiley & Sons: New York, 1997.
- [40] O.C. Zienkiewicz and R.L. Taylor. *The finite element method. Vol. I. Basic formulations and linear problems* (4th edn). McGraw-Hill: London, 1989.
- [41] W.H. Press, S.A. Teukolsky, W.T. Vetterling, and B.P. Flannery. *Numerical Recipes in C - The Art of Scientific Computing* (2nd edn). Cambridge University Press, 1992.
- [42] A. Cardona, I. Klapka, and M. Géradin. Design of a new finite element programming environment. *Engineering Computations* 1994; **11**:365–381.
- [43] T.R. Wilson. The design and construction of flexible manipulators. Master’s thesis, Georgia Institute of Technology, 1986.

- [44] J.D. Huggins. Experimental verification of a model of a two-link flexible, lightweight manipulator. Master's thesis, Georgia Institute of Technology, 1988.
- [45] J.W. Lee. *Dynamic Analysis and Control of Lightweight Manipulators With Flexible Parallel Link Mechanism*. PhD thesis, Georgia Institute of Technology, 1990.
- [46] O. Brüls, P. Duysinx, and J.-C. Golinval. A model reduction method for the control of rigid mechanisms. *Multibody System Dynamics*, in press:–, 2006.